Utrecht University

Department of Earth Sciences

Master's Thesis

March 9, 2015

Seismic interferometry by cross-convolution

Jasper Ploegstra

Supervisors:

Dr. Elmer Ruigrok

Department of Earth Sciences, Utrecht University, Utrecht, The Netherlands

Dr. Hanneke Paulssen

Department of Earth Sciences, Utrecht University, Utrecht, The Netherlands

Abstract

Seismic interferometry by cross-correlating recordings from transient or noise sources is often used to retrieve the Green's function between two receivers. However, in order to do this, a configuration is required where the sources surround both receivers. Interferometry by cross-correlation fails to work when such a configuration of sources cannot be achieved. Seismic interferometry by cross-convolution can be applied instead when only one of the receivers is surrounded by the source distribution. In this work, it is investigated whether the convolution approach can be used to retrieve the Green's function using recordings from transient sources or noise recordings. First, it is shown that the reciprocity theorem leads to a Green's function representation. This representation can be applied to retrieve the Green's function between two receivers using the convolution of the corresponding recordings. When the sources are transient, the convolutions have to be corrected for the source time function before integration over the source positions. When the source time function is known, the convolution approach is suitable for the retrieval of the Green's function from earthquake recordings. For uncorrelated noise sources, the convolution of the noise recordings provides no information about the Green's function between the receivers. Therefore, the cross-convolution approach cannot be used to retrieve the Green's function from noise recordings.

Keywords

Seismology - Interferometry - Convolution - Green's function - Uncorrelated noise

Contents

1 Introduction

Seismic waves are often used to gain information about the deep structure of the Earth. The seismic signal that is measured by a seismometer typically contains the impulse response, or Green's function, between the receiver and the source convolved with a source-time function. This Green's function provides information about the subsurface of the Earth. A problem arises when this method is used when there are no seismic sources present in a given area. Seismic interferometry can potentially overcome this problem.

In seismic interferometry the interference of seismic waves is used in order to obtain information about the stationary path between two receivers. When two seismometers are surrounded by a source distribution, the Green's function between the two receivers can be retrieved from the measurements. This is done by stacking the cross-correlation of the observations at the receivers for each source (for a tutorial on seismic interferometry the reader is referred to Wapenaar et al. (2010)). This technique can also be applied to noise recordings (e.g. Shapiro and Campillo, 2004 and Curtis et al., 2006). For noise sources, in the ideal case, the stacking over source locations is implicitly accounted for when the signals are measured for a sufficiently long time. Hence, the cross-correlation of two noise recordings provides an approximation of the Green's function between the two recorders.

The cross-correlation approach cannot be used when the receivers are not surrounded by the sources. In some situations one of the receivers is surrounded by a source distribution, whereas the other receiver is outside of this distribution. An example of such a configuration is when microseism (seismic waves resulting from interactions of ocean waves with the Earth) recordings are used where one receiver is located in the United Kingdom and the other receiver in the Netherlands. Slob et al. (2007) showed that for electromagnetic waves convolutions can be used to obtain the Green's function between the receivers when the sources are distributed as described above. Halliday and Curtis (2009) have showed that seismic interferometry using convolutions is effective for scattered surface waves in attenuating elastic media.

In this work the goal is to retrieve the surface wave portion of the acoustic and elastodynamic Green's functions using cross-convolutions in lossless fluid and solid media, respectively. In order to do so an expression is derived which retrieves the Green's function between two receivers using the convolution of the recordings at those receivers. First, the acoustic and elastodynamic Green's function representations are derived from the reciprocity relation in both fluid and solid media, respectively. It is then investigated how this representation can be implemented for the application of transient and noise source data.

2 Interferometry for acoustic Green's functions

In this section an expression is derived for acoustic Green's functions in arbitrarily inhomogeneous fluid media which can be used in the context of interferometry. In this derivation, a similar approach is used as in Wapenaar and Fokkema (2006). Wapenaar and Fokkema (2006) use a configuration in which two receivers are surrounded by a source distribution, whereas in this work the receivers are located at either side of the source distribution. Because of this source-receiver configuration a reciprocity relation of the convolution type is used whereas Wapenaar and Fokkema (2006) use the reciprocity relation of the correlation type as the starting point for deriving an interferometric relation.

2.1 Acoustic reciprocity theorem

The following definition of the temporal Fourier transform of a space- and time-dependent function $g(\mathbf{x}, t)$ is used:

$$\hat{g}(\mathbf{x}, \omega) = \int_{-\infty}^{\infty} e^{-i\omega t} g(\mathbf{x}, t) dt, \tag{1}$$

where i is the imaginary unit, ω the angular frequency and $\mathbf{x}$ denotes a position vector. All quantities used throughout this work are summarized in table 1. Symbols denoted with a hat represent quantities in the frequency domain. In arbitrary, inhomogeneous fluid media, the linearized Stokes equation in the space-frequency domain is given by

$$i\omega\rho\hat{v}_i + \partial_i\hat{p} = \hat{f}_i, \tag{2}$$

Symbol	Quantity	Unit
α	Angle between the ray and the normal vector	rad
β	Angle between the S-wave propagation direction and the normal vector	rad
δ_{ij}	Kronecker delta	-
$\delta(x)$	Dirac delta function	-
ε_{ijk}	Levi-Civita tensor	-
θ	Source coordinate	rad
θ_0	Stationary point location	rad
κ	Compressibility	Pa^{-1}
λ	Lamé's first parameter	Pa
μ	Lamé's second parameter	Pa
ρ	Density	$\mathrm{kg\ m}^{-3}$
τ_{ij}	Stress tensor	Pa
ϕ	P-wave potential	$\mathrm{J\ m}^{-3}$
$\hat{\Phi}$	Phase function	-
ψ	S-wave potential	$\mathrm{J\ m}^{-3}$
ω	Angular frequency	$\mathrm{rad\ s}^{-1}$
A	Amplitude function	(varies)
c_{ijkl}	Stiffness tensor	Pa
$\mathbb{D}$	Integration domain	m^3
$\mathbf{f}$	External volume force density	$\mathrm{N\ m}^{-3}$
G	Green's function	(varies)
h_{ij}	External deformation rate density	s^{-1}
i	Imaginary unit	-
k	Wavenumber	m^{-1}
$\hat{N}$	Angular frequency spectrum of the noise source	m^{-2}
$\mathbf{n}$	Normal vector pointing outward from the surface $\partial\mathbb{D}$	-
p	Acoustic pressure	Pa
q	Volume injection rate density	s^{-1}
r	Radius	m
$\hat{R}$	Autocorrelation of the source wavelet	-
$\lvert\mathbf{r}\rvert$	Distance between the source to the receiver	m
$\hat{s}$	Angular frequency spectrum of the source wavelet	-
$\hat{S}$	Autoconvolution of the source wavelet	-
s_{ijkl}	Compliance	Pa^{-1}
t	Time	s
v	Wave velocity	$\mathrm{m\ s}^{-1}$
v_p	P-wave velocity	$\mathrm{m\ s}^{-1}$
v_s	S-wave velocity	$\mathrm{m\ s}^{-1}$
$\mathbf{v}$	Particle velocity	$\mathrm{m\ s}^{-1}$
$\mathbf{x}$	Position	m
x_i	Dipole direction	-
$\partial\mathbb{D}$	Boundary of the integration domain	m^2
∂_i	Spatial derivative in the x_i direction	m^{-1}

Table 1: Description of the quantities and the units corresponding to symbols used in this work.

and the stress-strain relation

$$i\omega\kappa\hat{p} + \partial_i\hat{v}_i = \hat{q} \tag{3}$$

where $\hat{p}(\mathbf{x},\omega)$ is the acoustic pressure, $\hat{v}_i(\mathbf{x},\omega)$ is the i^{th} component of the particle velocity, $\rho(\mathbf{x})$ is the mass density, $\kappa(\mathbf{x})$ is the compressibility, $\hat{f}_i(\mathbf{x},\omega)$ the external force density and $\hat{q}(\mathbf{x},\omega)$ is a source distribution

of volume injection rate density. Note that Einstein's summation convention applies to repeated indices. Furthermore the interaction quantity is defined as

$$\partial_i \left(\hat{p}_A \hat{v}_{i,B} - \hat{v}_{i,A} \hat{p}_B \right). \tag{4}$$

This interaction quantity describes the interaction between two independent acoustic states A and B. States A and B are defined by source and medium properties. Note that multiplication in the frequency domain corresponds to convolution in the time domain. An arbitrary domain $\mathbb{D}$ with boundary $\partial\mathbb{D}$ and outward pointing normal $\mathbf{n}$ is defined (figure 1). Integrating the interaction quantity over this domain and applying the divergence theorem yields

$$\int_{\mathbb{D}} \partial_i \left(\hat{p}_A \hat{v}_{i,B} - \hat{v}_{i,A} \hat{p}_B \right) d^3\mathbf{x} = \oint_{\partial\mathbb{D}} \left(\hat{p}_A \hat{v}_{i,B} - \hat{v}_{i,A} \hat{p}_B \right) n_i d^2\mathbf{x}. \tag{5}$$

The products in the left-hand side integral are expanded using the product rule; rewriting the terms for states A and B using equations (2) and (3) results in

$$\int_{\mathbb{D}} \left(\hat{p}_A \hat{q}_B - \hat{v}_{i,A} \hat{f}_{i,B} - \hat{q}_A \hat{p}_B + \hat{f}_{i,A} \hat{v}_{i,B} \right) d^3\mathbf{x} = \oint_{\partial\mathbb{D}} \left(\hat{p}_A \hat{v}_{i,B} - \hat{v}_{i,A} \hat{p}_B \right) n_i d^2\mathbf{x}. \tag{6}$$

This is a reciprocity theorem of the convolution type (Wapenaar and Fokkema, 2006).

2.2 Interferometry for acoustic pressure

The sources are chosen as point sources of volume injection rate according to

$$\hat{q}_A(\mathbf{x}, \omega) = \delta(\mathbf{x} - \mathbf{x}_A) \tag{7}$$

and

$$\hat{q}_B(\mathbf{x}, \omega) = \delta(\mathbf{x} - \mathbf{x}_B). \tag{8}$$

In both states the external force density sources are absent such that

$$\hat{f}_{i,A}(\mathbf{x}, \omega) = 0 \tag{9}$$

and

$$\hat{f}_{i,B}(\mathbf{x}, \omega) = 0. \tag{10}$$

A configuration is chosen such that $\mathbf{x}_A$ and $\mathbf{x}_B$ are located inside and outside $\mathbb{D}$ respectively (figure 1). The acoustic Green's function is defined to be equal to the acoustic pressure and the particle velocity is expressed in terms of the acoustic Green's function using equation (2). This yields

$$\hat{p}_A(\mathbf{x}, \omega) := \hat{G}(\mathbf{x}, \mathbf{x}_A, \omega), \tag{11}$$

$$\hat{p}_B(\mathbf{x}, \omega) := \hat{G}(\mathbf{x}, \mathbf{x}_B, \omega), \tag{12}$$

$$\hat{v}_{i,A}(\mathbf{x}, \omega) = -(i\omega\rho(\mathbf{x}))^{-1} \partial_i \hat{G}(\mathbf{x}, \mathbf{x}_A, \omega) \tag{13}$$

and

$$\hat{v}_{i,B}(\mathbf{x}, \omega) = -(i\omega\rho(\mathbf{x}))^{-1} \partial_i \hat{G}(\mathbf{x}, \mathbf{x}_B, \omega). \tag{14}$$

The first argument of the Green's function denotes the receiver location and the second argument denotes the source location. It follows from these choices for the Green's functions and the sources, and substitution of equations (7), (11) and (13) into (3) that $\hat{G}(\mathbf{x}, \mathbf{x}_A, \omega)$ obeys the forced wave equation

$$\partial_i \rho^{-1} \partial_i \hat{G}_A + \frac{\omega^2}{\rho v^2} \hat{G}_A = -i\omega\delta(\mathbf{x} - \mathbf{x}_A), \tag{15}$$

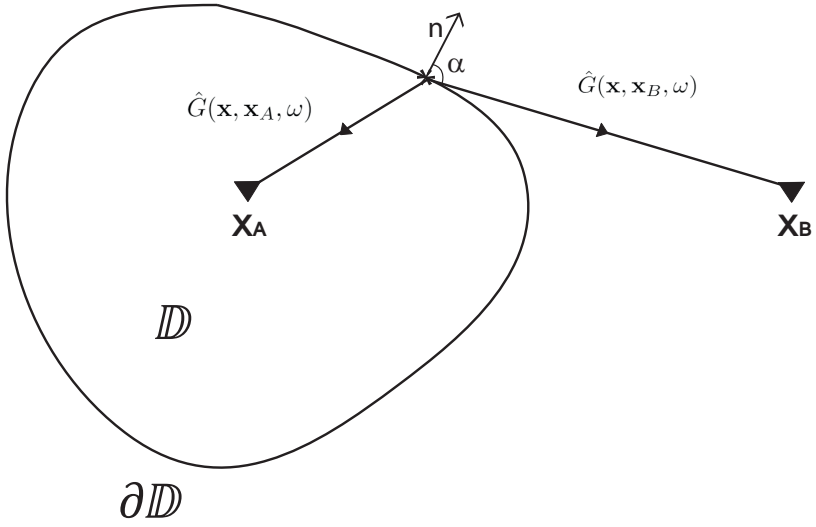

Figure 1: The domain $\mathbb{D}$ with boundary $\partial\mathbb{D}$ and outward pointing normal $\mathbf{n}$. The Green's functions $\hat{G}(\mathbf{x}_A, \mathbf{x}, \omega)$ and $\hat{G}(\mathbf{x}_B, \mathbf{x}, \omega)$ are indicated. The source is denoted by $*$. The ray makes an angle α with the normal vector $\mathbf{n}$.

where G_A is an abbreviated notation for the Green's function $\hat{G}(\mathbf{x}, \mathbf{x}_A, \omega)$ and v is the wave velocity in the medium. Substituting equations (7)-(14) into (6) yields

$$\begin{aligned} &\int_{\mathbb{D}} \hat{G}(\mathbf{x}, \mathbf{x}_A, \omega)\delta(\mathbf{x} - \mathbf{x}_B) - \hat{G}(\mathbf{x}, \mathbf{x}_B, \omega)\delta(\mathbf{x} - \mathbf{x}_A)d^3\mathbf{x} = \\ &\oint_{\partial\mathbb{D}} -\frac{1}{i\omega\rho(\mathbf{x})}\Big(\hat{G}(\mathbf{x}, \mathbf{x}_A, \omega)\partial_i\hat{G}(\mathbf{x}, \mathbf{x}_B, \omega) - (\partial_i\hat{G}(\mathbf{x}, \mathbf{x}_A, \omega))\hat{G}(\mathbf{x}, \mathbf{x}_B, \omega)\Big)\, n_i d^2\mathbf{x}. \end{aligned} \tag{16}$$

Equation (16) contains both monopole and dipole responses denoted by $\hat{G}$ and $\partial_i\hat{G}n_i$, respectively. Because $\mathbf{x}_B$ is chosen outside of the domain $\mathbb{D}$, $\delta(\mathbf{x} - \mathbf{x}_B)$ is zero everywhere in the domain. Applying this and the shifting property of the delta function to equation (16) gives

$$\begin{aligned} \hat{G}(\mathbf{x}_A, \mathbf{x}_B, \omega) = \oint_{\partial\mathbb{D}} \frac{1}{i\omega\rho(\mathbf{x})}\Big(&\hat{G}(\mathbf{x}, \mathbf{x}_A, \omega)\partial_i\hat{G}(\mathbf{x}, \mathbf{x}_B, \omega) \\ &- (\partial_i\hat{G}(\mathbf{x}, \mathbf{x}_A, \omega))\hat{G}(\mathbf{x}, \mathbf{x}_B, \omega)\Big) n_i d^2\mathbf{x}. \end{aligned} \tag{17}$$

Using the source-receiver reciprocity relation $\hat{G}(\mathbf{x}, \mathbf{x}', \omega) = \hat{G}(\mathbf{x}', \mathbf{x}, \omega)$ (Wapenaar and Fokkema, 2006) the following equation is obtained

$$\begin{aligned} \hat{G}(\mathbf{x}_A, \mathbf{x}_B, \omega) = \oint_{\partial\mathbb{D}} \frac{1}{i\omega\rho(\mathbf{x})}\Big(&\hat{G}(\mathbf{x}_A, \mathbf{x}, \omega)\partial_i\hat{G}(\mathbf{x}_B, \mathbf{x}, \omega) \\ &- (\partial_i\hat{G}(\mathbf{x}_A, \mathbf{x}, \omega))\hat{G}(\mathbf{x}_B, \mathbf{x}, \omega)\Big) n_i d^2\mathbf{x}. \end{aligned} \tag{18}$$

Equation (18) describes how the Green's function between the receivers at $\mathbf{x}_A$ and $\mathbf{x}_B$ can be retrieved from the responses measured at the two receivers. In order to do so, the monopole response measured at $\mathbf{x}_A$ has to be convolved with the dipole response measured at $\mathbf{x}_B$ for each source on $\partial\mathbb{D}$ and vice versa. To obtain the Green's function between the receivers, the difference of these convolutions has to be stacked over the source locations. Note that equation (18) provides the exact Green's function for any lossless fluid medium and is therefore the

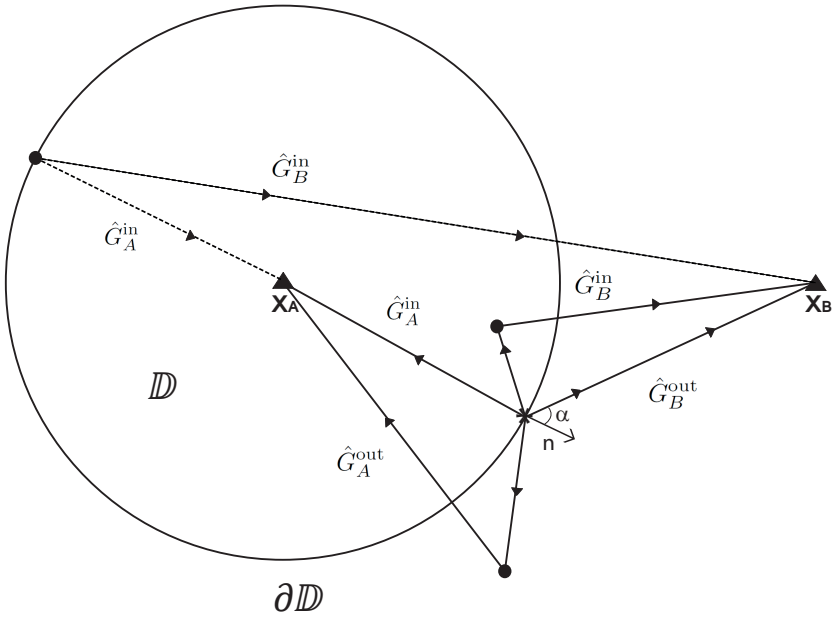

Figure 2: The inward and outward traveling part of the Green's function. The total Green's function for a given source (denoted by $*$) on $\partial\mathbb{D}$ is the sum of the inward and outward traveling parts. In order for $\hat{G}_A^{\text{out}}$ and $\hat{G}_B^{\text{in}}$ to exist, scatterers (denoted by $\bullet$) have to be present. The ray paths for the different Green's functions are shown by solid lines. Contributions to $\hat{G}_B^{\text{in}}$ can also result from a direct wave originated at the far end of $\partial\mathbb{D}$ (ray path indicated with a dashed line).

basis for seismic interferometry by cross-convolution. The choice of the volume $\mathbb{D}$ is not constrained as long as it contains $\mathbf{x}_A$ and not $\mathbf{x}_B$. A numerical example is given in appendix A, which illustrates how equation (18) works.

2.3 Simplification of the convolution integral

Expression (18) is not efficient for the retrieval of the Green's function between the two receivers. This is mainly because the integral contains monopole and dipole responses denoted by $\hat{G}$ and $\partial_i\hat{G}n_i$, respectively, which must be known for all sources on $\partial\mathbb{D}$. Furthermore, the computation of a convolution product can become time consuming if the measured signals are large. In this section the amount of convolution products in expression (18) is reduced from two to one. To make expression (18) more manageable for uses in seismic interferometry the wavefield is decomposed into a inward and outward propagating part (figure 2) according to

$$\hat{G}_A = \hat{G}_A^{\text{in}} + \hat{G}_A^{\text{out}}. \tag{19}$$

For convenience the explicit notation of the dependence of the Green's functions is temporarily omitted by using $\hat{G}_A$ to denote $\hat{G}(\mathbf{x}_A, \mathbf{x}, \omega)$ and $\hat{G}_B$ to denote $\hat{G}(\mathbf{x}_B, \mathbf{x}, \omega)$. Applying expression (19) to equation (18) results in

$$\begin{aligned}\hat{G}(\mathbf{x}_A, \mathbf{x}_B, \omega) = \oint_{\partial\mathbb{D}} \frac{1}{i\omega\rho(\mathbf{x})}\Big((\hat{G}_A^{\text{in}} + \hat{G}_A^{\text{out}})(\partial_i\hat{G}_B^{\text{in}} + \partial_i\hat{G}_B^{\text{out}}) \\ - (\partial_i\hat{G}_A^{\text{in}} + \partial_i\hat{G}_A^{\text{out}})(\hat{G}_B^{\text{in}} + \hat{G}_B^{\text{out}})\Big)n_i d^2\mathbf{x}.\end{aligned} \tag{20}$$

For high frequencies, the spatial derivatives of the Green's functions can be approximated by multiplying the Green's function with $\mp\frac{i\omega}{v(\mathbf{x})}|\cos(\alpha(\mathbf{x}))|$ where $\alpha(\mathbf{x})$ is the angle between the ray and the normal vector (figure

2), the minus sign corresponds to the inward propagating waves. The main contributions to the integral originate from stationary points on $\partial\mathbb{D}$, i.e. the locations where $|\cos(\alpha(\mathbf{x}))|$ are equal for $\hat{G}_A$ and $\hat{G}_B$. In sections 3.1 and 3.2 it is shown in an example that the stationary points are indeed the locations where $|\cos(\alpha(\mathbf{x}))|$ is equal for $\hat{G}_A$ and $\hat{G}_B$. This means that products of waves that travel inward or outward in both states cancel and products of inward traveling waves in one state and outward traveling waves in the other state give equal contributions to the integral. Therefore, equation (20) can be rewritten as

$$\hat{G}(\mathbf{x}_A,\mathbf{x}_B,\omega) = \oint_{\partial\mathbb{D}} \frac{-2}{i\omega\rho(\mathbf{x})}\Big((\partial_i\hat{G}_A^{\text{in}})\hat{G}_B^{\text{out}} + (\partial_i\hat{G}_A^{\text{out}})\hat{G}_B^{\text{in}}\Big)n_i d^2\mathbf{x}. \tag{21}$$

Using expression (19) the following equation is obtained

$$(\partial_i\hat{G}_A^{\text{in}})\hat{G}_B^{\text{out}} + (\partial_i\hat{G}_A^{\text{out}})\hat{G}_B^{\text{in}} = (\partial_i\hat{G}_A)\hat{G}_B - (\partial_i\hat{G}_A^{\text{in}})\hat{G}_B^{\text{in}} - (\partial_i\hat{G}_A^{\text{out}})\hat{G}_B^{\text{out}}. \tag{22}$$

Combining equations (21) and (22) yields

$$\hat{G}(\mathbf{x}_A,\mathbf{x}_B,\omega) + \oint_{\partial\mathbb{D}} \frac{-2}{i\omega\rho(\mathbf{x})}\Big((\partial_i\hat{G}_A^{\text{in}})\hat{G}_B^{\text{in}} + (\partial_i\hat{G}_A^{\text{out}})\hat{G}_B^{\text{out}}\Big)n_i d^2\mathbf{x} = \oint_{\partial\mathbb{D}} \frac{-2}{i\omega\rho(\mathbf{x})}(\partial_i\hat{G}(\mathbf{x}_A,\mathbf{x},\omega))\hat{G}(\mathbf{x}_B,\mathbf{x},\omega)n_i d^2\mathbf{x}. \tag{23}$$

The integral on the left-hand side of equation (23) adds spurious terms to the reconstructed Green's function. It contains convolution products of waves that reach one receiver via a scatterer and waves that travel directly to the other receiver. Also, the integral contains the contributions of waves that travel inward in both states. These contributions result from those points on $\partial\mathbb{D}$ where the convolutions provide no information on the stationary path between $\mathbf{x}_A$ and $\mathbf{x}_B$. When the medium contains scatterers, the convolutions of scattered waves with direct waves do not integrate coherently when $\partial\mathbb{D}$ is an irregular surface. This is the case when the sources are randomly distributed. No scattering can occur, when the medium is laterally homogeneous. Hence, the contributions from scatterers in the left-hand side integral of equation (23) go to zero, though the contributions from waves traveling inward for both states remain. Therefore, equation (23) in laterally homogeneous media can be written as

$$\hat{G}(\mathbf{x}_A,\mathbf{x}_B,\omega) + \oint_{\partial\mathbb{D}} \frac{-2}{i\omega\rho(\mathbf{x})}(\partial_i\hat{G}_A^{\text{in}})\hat{G}_B^{\text{in}}n_i d^2\mathbf{x} = \oint_{\partial\mathbb{D}} \frac{-2}{i\omega\rho(\mathbf{x})}(\partial_i\hat{G}(\mathbf{x}_A,\mathbf{x},\omega))\hat{G}(\mathbf{x}_B,\mathbf{x},\omega)n_i d^2\mathbf{x}. \tag{24}$$

The contributions from these waves are separated in time from the reconstructed Green's function when the distance of $\mathbf{x}_A$ to the far side of $\partial\mathbb{D}$ is sufficiently large, as will be shown in an example in section 3. When $\partial\mathbb{D}$ is a sphere with a very large radius, all rays are perpendicular to $\partial\mathbb{D}$ and the dipole responses can be approximated using

$$\partial_i\hat{G}(\mathbf{x}_A,\mathbf{x},\omega)n_i \approx -\frac{i\omega}{v}\hat{G}(\mathbf{x}_A,\mathbf{x},\omega) \tag{25}$$

to get

$$\hat{G}(\mathbf{x}_A,\mathbf{x}_B,\omega) + \frac{2}{\rho v}\oint_{\partial\mathbb{D}} \hat{G}_A^{\text{in}}\hat{G}_B^{\text{in}}d^2\mathbf{x} = \frac{2}{\rho v}\oint_{\partial\mathbb{D}} \hat{G}(\mathbf{x}_A,\mathbf{x},\omega)\hat{G}(\mathbf{x}_B,\mathbf{x},\omega)d^2\mathbf{x}. \tag{26}$$

2.4 Transient sources

The results obtained in the previous sections are only valid when the sources are impulsive point sources of volume injection rate (equations (7) and (8)). When this method is applied to real data, the sources are no longer impulsive point sources but transient sources which generate a wavelet $s(\mathbf{x},t)$ (Wapenaar and Fokkema, 2006). The observed quantity, in this case the acoustic pressure, at the receivers at $\mathbf{x}_A$ and $\mathbf{x}_B$ is the Green's function convolved with the source wavelet. In the frequency domain this is expressed as

$$\hat{p}^{\text{obs}}(\mathbf{x}_A,\mathbf{x},\omega) = \hat{G}(\mathbf{x}_A,\mathbf{x},\omega)\hat{s}(\mathbf{x},\omega) \tag{27}$$

for the station at $\mathbf{x}_A$ and

$$\hat{p}^{\text{obs}}(\mathbf{x}_B,\mathbf{x},\omega) = \hat{G}(\mathbf{x}_B,\mathbf{x},\omega)\hat{s}(\mathbf{x},\omega) \tag{28}$$

for the station at $\mathbf{x}_B$, where $\hat{s}(\mathbf{x},\omega)$ is the angular frequency spectrum of the wavelet. This is applied to equation (26) to obtain

$$\hat{G}(\mathbf{x}_A,\mathbf{x}_B,\omega)+\frac{2}{\rho v}\oint_{\partial\mathbb{D}}\frac{1}{\hat{S}(\mathbf{x},\omega)}\hat{p}_A^{\text{in}}\hat{p}_B^{\text{in}}d^2\mathbf{x}=\frac{2}{\rho v}\oint_{\partial\mathbb{D}}\frac{1}{\hat{S}(\mathbf{x},\omega)}\hat{p}^{\text{obs}}(\mathbf{x}_A,\mathbf{x},\omega)\hat{p}^{\text{obs}}(\mathbf{x}_B,\mathbf{x},\omega)d^2\mathbf{x}, \tag{29}$$

where $\hat{S}(\mathbf{x},\omega)$ is the autoconvolution of the source wavelet. The spectrum of the wavelet can be split in an amplitude spectrum and a phase spectrum according to $\hat{s}(\mathbf{x},\omega)=\hat{A}(\mathbf{x},\omega)e^{i\hat{\Phi}(\mathbf{x},\omega)}$. Note that the phase spectrum is a function of the source activation time. The autoconvolution and autocorrelation of the source wavelet are defined by $\hat{S}(\mathbf{x},\omega):=(\hat{s}(\mathbf{x},\omega))^2=(\hat{A}(\mathbf{x},\omega))^2e^{2i\hat{\Phi}(\mathbf{x},\omega)}$ and $\hat{R}(\mathbf{x},\omega):=\hat{s}(\mathbf{x},\omega)\hat{s}^*(\mathbf{x},\omega)=(\hat{A}(\mathbf{x},\omega))^2$, respectively. Note that in the autoconvolution of the source wavelet, the phase term adds up whereas it cancels in the autocorrelation. Therefore, in order to evaluate the integral in equation (29) the amplitude spectrum and the phase spectrum must be known for each source on $\partial\mathbb{D}$. The largest contributions to the integral in equation (29) come from near the stationary points on $\partial\mathbb{D}$. Therefore it is only required to know $\hat{S}(\mathbf{x},\omega)$ accurately for sources near the stationary point.

2.5 Noise sources

When uncorrelated noise sources are used instead of transient sources a problem arises when using equation (29). This is explained by applying the same analysis as done in Wapenaar and Fokkema (2006).
Suppose $\partial\mathbb{D}$ consists of a large amount of uncorrelated noise sources with identical power spectra. If the spectrum of the noise is given by $\hat{N}(\mathbf{x},\omega)$ and all noise sources act simultaneously, the observed acoustic pressure at $\mathbf{x}_A$ and at $\mathbf{x}_B$ are given by

$$\hat{p}^{\text{obs}}(\mathbf{x}_A,\omega)=\oint_{\partial\mathbb{D}}\hat{G}(\mathbf{x}_A,\mathbf{x},\omega)\hat{N}(\mathbf{x},\omega)d^2\mathbf{x} \tag{30}$$

and

$$\hat{p}^{\text{obs}}(\mathbf{x}_B,\omega)=\oint_{\partial\mathbb{D}}\hat{G}(\mathbf{x}_B,\mathbf{x}',\omega)\hat{N}(\mathbf{x}',\omega)d^2\mathbf{x}', \tag{31}$$

respectively. The spatial average of convolutions of the responses from two noise sources at $\mathbf{x}$ and $\mathbf{x}'$ follows the relation

$$\langle\hat{N}(\mathbf{x},\omega)\hat{N}(\mathbf{x}',\omega)\rangle=0. \tag{32}$$

$\langle\cdot\rangle$ represents spatial ensemble averaging, which is usually replaced by measuring the signals over a large time interval and taking the average (e.g. Wapenaar et al., 2011 and Slob et al., 2007). When the spatial ensemble average over source locations of the observed acoustic pressure is taken and combined with equations (30)-(32) the result is

$$\langle\hat{p}^{\text{obs}}(\mathbf{x}_A,\omega)\hat{p}^{\text{obs}}(\mathbf{x}_B,\omega)\rangle=0. \tag{33}$$

This result shows that the measurements of acoustic pressure resulting from simultaneously active uncorrelated noise sources cannot be used to obtain the Green's function between the two receivers using interferometry by convolution. In deriving this expression, it is assumed that the noise sources act at the same time, which is not always the case. For some noise sources it is a better assumption that the sources are active in succession. A microseism is an example of such a noise source. Miscroseisms are seismic noise resulting from the interaction of ocean waves with the solid Earth. The dominating source will be at a different location each day, depending on the weather conditions. In this case the Green's function can be retrieved using expression (29). The source time functions for microseisms are long and generally unknown, hence the correction for the autoconvolution cannot be made properly. In either case, the Green's function cannot be retrieved using the autoconvolution of seismic noise recordings.

3 Interferometry examples

In this section the validity of equation (24) is shown by evaluating the right-hand side integral for Green's functions that are solutions to the acoustic wave equation for a vertical line source. Besides that, it is shown numerically that equation (29) is valid for two different configurations of $\partial\mathbb{D}$.

3.1 An analytical example

For a homogeneous lossless fluid medium, the far-field approximations of the solutions to the acoustic wave equation for a vertical line source at $\mathbf{x}_S = (x_1, x_2)^T = (0,0)^T$ in the frequency domain are given by K. Wapenaar (personal communication, October, 2014). The solutions for a monopole and dipole source are

$$\hat{G}(\mathbf{x}, \mathbf{x}_S, \omega) = \frac{e^{-i(\omega|\mathbf{r}|/v + \frac{\pi}{4})}}{\sqrt{8\pi\omega|\mathbf{r}|/v}} \tag{34}$$

and

$$\partial_i \hat{G}(\mathbf{x}, \mathbf{x}_S, \omega) n_i = \frac{x_i n_i}{|\mathbf{r}|} \frac{\omega}{v} \frac{e^{-i(\omega|\mathbf{r}|/v - \frac{\pi}{4})}}{\sqrt{8\pi\omega|\mathbf{r}|/v}}, \tag{35}$$

respectively. $\mathbf{r}$ is the position vector pointing from the source to the receiver and $\frac{x_i}{|\mathbf{r}|}$ denotes the normalized direction of the dipole. However, these Green's functions obey the following wave equation:

$$\partial_i \partial_i \hat{G} + \frac{\omega^2}{v^2} \hat{G} = -\delta(\mathbf{x} - \mathbf{x}_S), \tag{36}$$

which is inconsistent with the wave equation that was used in the derivation of expression (24). To solve this inconsistency the Green's functions obtained from K. Wapenaar (personal communication, October, 2014) have to be multiplied by a factor $i\omega\rho$. This results in

$$\hat{G}(\mathbf{x}, \mathbf{x}_S, \omega) = i\omega\rho \frac{e^{-i(\omega|\mathbf{r}|/v + \frac{\pi}{4})}}{\sqrt{8\pi\omega|\mathbf{r}|/v}} \tag{37}$$

and

$$\partial_i \hat{G}(\mathbf{x}, \mathbf{x}_S, \omega) n_i = i\omega\rho \frac{x_i n_i}{|\mathbf{r}|} \frac{\omega}{v} \frac{e^{-i(\omega|\mathbf{r}|/v - \frac{\pi}{4})}}{\sqrt{8\pi\omega|\mathbf{r}|/v}} \tag{38}$$

for the monopole and dipole responses in the frequency domain respectively. In this case sources are considered at locations $\mathbf{x}_S(\mathbf{x})$ located on an origin centered circle with radius r and outward pointing normal $\mathbf{n}$. These signals are measured at stations $\mathbf{x}_A$ at the center of the circle and $\mathbf{x}_B$ at a location outside the circle (figure 3). The Fourier transforms of the dipole response measured at receiver A and the monopole response measured a receiver B are defined as

$$\partial_i \hat{G}(\mathbf{x}_A, \mathbf{x}_S, \omega) n_i = -\frac{i\omega^2\rho}{v} \frac{e^{-i(\omega|\mathbf{r}_A(\theta)|/v - \frac{\pi}{4})}}{\sqrt{8\pi\omega|\mathbf{r}_A(\theta)|/v}} \tag{39}$$

and

$$\hat{G}(\mathbf{x}_B, \mathbf{x}_S, t) = i\omega\rho \frac{e^{-i(\omega|\mathbf{r}_B(\theta)|/v + \frac{\pi}{4})}}{\sqrt{8\pi\omega|\mathbf{r}_B(\theta)|/v}}, \tag{40}$$

respectively.
Here $|\mathbf{r}_A(\theta)| = r$ and $|\mathbf{r}_B(\theta)| = |\mathbf{x}_B - \mathbf{x}_S| = \sqrt{|\mathbf{x}_B|^2 + r^2 + 2|\mathbf{x}_B| r\cos(\theta)}$ are the distances of the sources to receivers. First, the Green's function between receivers at $\mathbf{x}_A$ and $\mathbf{x}_B$ is calculated using expression (24). Note that a large number of equidistant sources on $\partial\mathbb{D}$ is required for equation (24) to be valid. For easier reference in the future, the right-hand side of equation (24) is from now on renamed as

$$J := \oint_{\partial\mathbb{D}} \frac{-2}{i\omega\rho} (\partial_i \hat{G}(\mathbf{x}_A, \mathbf{x}, \omega)) \hat{G}(\mathbf{x}_B, \mathbf{x}, \omega) n_i d^2\mathbf{x}. \tag{41}$$

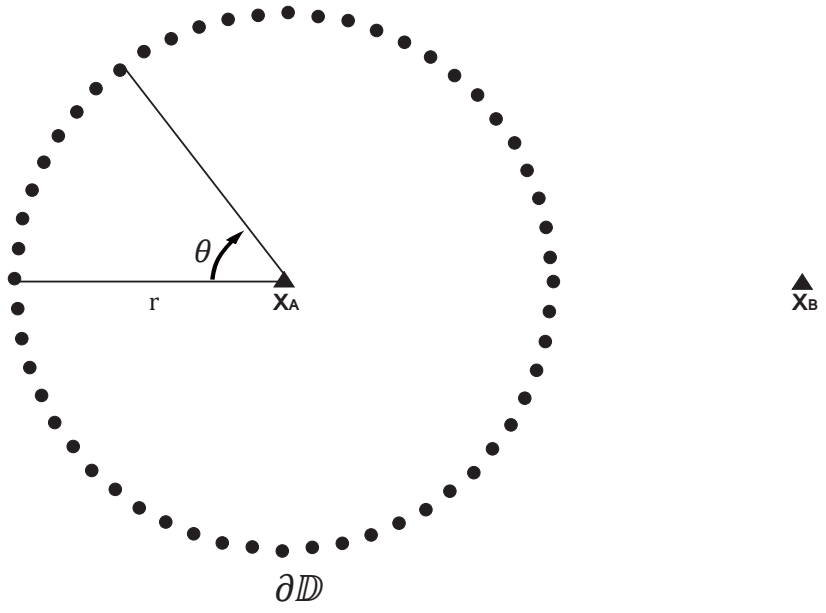

Figure 3: The configuration used in the examples. Sources (denoted by •) are located on $\partial\mathbb{D}$, which is a circle with radius r, with $\mathbf{x}_A \in \mathbb{D}$ at the center of the circle and $\mathbf{x}_B \notin \mathbb{D}$. The angle θ is measured clockwise from the horizontal.

The surface integral over Cartesian coordinates $d^2\mathbf{x}$ is transformed to an integral over cylindrical coordinate θ (e.g., Boas, 2006):

$$J = \int_0^{2\pi} \frac{-2}{i\omega\rho} \partial_i \hat{G}(\mathbf{x}_A, \mathbf{x}_S, \omega) n_i \hat{G}(\mathbf{x}_B, \mathbf{x}_S, \omega) r d\theta. \tag{42}$$

Using expressions (39) and (40) for the Fourier transforms of the Green's functions and using $k = \frac{\omega}{v}$, J becomes

$$J = \frac{-2}{i\omega\rho} \int_0^{2\pi} -(i\omega\rho)^2 kr \frac{\exp\left(-i\left(kr - \pi/4\right)\right)}{\sqrt{8\pi kr}} \frac{\exp\left(-i\left(k\sqrt{|\mathbf{x}_B|^2 + r^2 + 2|\mathbf{x}_B| r\cos(\theta)} + \pi/4\right)\right)}{\sqrt{8\pi k\sqrt{|\mathbf{x}_B|^2 + r^2 + 2|\mathbf{x}_B| r\cos(\theta)}}} d\theta. \tag{43}$$

Rearranging the terms yields

$$J = i\omega\rho \int_0^{2\pi} \frac{r}{4\pi \sqrt[4]{r^2\left(|\mathbf{x}_B|^2 + r^2 + 2|\mathbf{x}_B| r\cos(\theta)\right)}} \exp\left(-i\left(k\left(r + \sqrt{|\mathbf{x}_B|^2 + r^2 + 2|\mathbf{x}_B| r\cos(\theta)}\right)\right)\right) d\theta. \tag{44}$$

This can be rewritten as

$$J = i\omega\rho \int_0^{2\pi} A(\theta) e^{ik\Phi(\theta)} d\theta \tag{45}$$

where

$$A(\theta) = \frac{r}{4\pi \sqrt[4]{r^2(|\mathbf{x}_B|^2 + r^2 + 2|\mathbf{x}_B| r\cos(\theta))}} \tag{46}$$

and

$$\Phi(\theta) = -\left(r + \sqrt{|\mathbf{x}_B|^2 + r^2 + 2|\mathbf{x}_B| r\cos(\theta)}\right). \tag{47}$$

The phase function Φ is stationary with respect to θ when $\Phi' = \frac{d\Phi}{d\theta} = 0$. In this case Φ' is given by

$$\Phi'(\theta) = \frac{|\mathbf{x}_B| r \sin(\theta)}{\sqrt{|\mathbf{x}_B|^2 + r^2 + 2|\mathbf{x}_B| r \cos(\theta)}}. \tag{48}$$

Hence, the stationary points are found for $\theta_0 = 0$ and $\theta_0 = \pi$. Note that at these stationary points the rays are parallel, or $|\cos(\alpha_A(\mathbf{x}))| = |\cos(\alpha_B(\mathbf{x}))|$. The integral expression J can be approximated around the stationary points for large values of $|k|$ using (see appendix C and Bleistein, 1984)

$$J \approx i\omega\rho \sqrt{\frac{2\pi}{|k\Phi''(\theta_0)|}} A(\theta_0) e^{i(k\Phi(\theta_0) + \mu\frac{\pi}{4})}, \tag{49}$$

with $\mu = \mathrm{sgn}(k\Phi''(\theta_0))$. $\mathrm{sgn}(x)$ denotes the signum function, which gives the sign of the argument x. In order to use equation (49), the second derivative of Φ with respect to θ has to be computed:

$$\Phi''(\theta) = \frac{|\mathbf{x}_B| r \cos(\theta)}{\sqrt{|\mathbf{x}_B|^2 + r^2 + 2|\mathbf{x}_B| r \cos(\theta)}} + \frac{|\mathbf{x}_B|^2 r^2 \sin^2(\theta)}{\left(|\mathbf{x}_B|^2 + r^2 + 2|\mathbf{x}_B| r \cos(\theta)\right)^{3/2}}. \tag{50}$$

Note that $\Phi''(\theta_0) > 0$ for $\theta_0 = 0$ and $\Phi''(\theta_0) < 0$ for $\theta_0 = \pi$. At the stationary points the phase function and its second derivative are given by

$$\Phi(0) = -(|\mathbf{x}_B| + 2r), \tag{51}$$

$$\Phi(\pi) = -|\mathbf{x}_B|, \tag{52}$$

$$\Phi''(0) = \frac{|\mathbf{x}_B| r}{|\mathbf{x}_B| + r}, \tag{53}$$

$$\Phi''(\pi) = \frac{|\mathbf{x}_B| r}{r - |\mathbf{x}_B|}, \tag{54}$$

and the amplitude function is given by

$$A(0) = \frac{r}{4\pi\sqrt{r(r + |\mathbf{x}_B|)}}, \tag{55}$$

$$A(\pi) = \frac{r}{4\pi\sqrt{r(|\mathbf{x}_B| - r)}}. \tag{56}$$

Combining equations (51)-(56) and (49) yields

$$\begin{aligned} J = {} & i\omega\rho \sqrt{\frac{2\pi}{k\frac{|\mathbf{x}_B| r}{|\mathbf{x}_B| + r}}} \frac{r}{4\pi\sqrt{r(|\mathbf{x}_B| + r)}} e^{i\left(-k(|\mathbf{x}_B| + 2r) + \frac{\pi}{4}\right)} \\ & + i\omega\rho \sqrt{\frac{2\pi}{k\frac{|\mathbf{x}_B| r}{|\mathbf{x}_B| - r}}} \frac{r}{4\pi\sqrt{r(|\mathbf{x}_B| - r)}} e^{-i\left(k|\mathbf{x}_B| + \frac{\pi}{4}\right)}. \end{aligned} \tag{57}$$

Equation (57) can be rewritten to

$$J = i\omega\rho \frac{1}{\sqrt{8\pi k|\mathbf{x}_B|}} \left(e^{i(-k(|\mathbf{x}_B| + 2r) + \frac{\pi}{4})} + e^{-i(k|\mathbf{x}_B| + \frac{\pi}{4})} \right). \tag{58}$$

The first exponential term in equation (58) is equal to the contributions of sources for which $\theta \approx 0$. The term resulting from this stationary point contains convolutions of inward traveling waves in both states. This implies that the first exponential term in equation (58) is a result from the integral on the left-hand side of equation (24). The travel time that can be extracted from this term is not useful, because it does not correspond to a physical wave. The contributions from this left-hand side integral are removed by splitting J into two parts:

$J = J_1 + J_2$. The contributions from the stationary point at $\theta = 0$ are included in J_1 and the contributions from the stationary point at $\theta = \pi$ are included in J_2. Therefore, the integral in equation (42) is replaced by

$$J_1 + J_2 = \frac{-2}{i\omega\rho} \int_0^{2\pi} \partial_i \hat{G}(\mathbf{x}_A, \mathbf{x}_S, \omega) n_i \hat{G}(\mathbf{x}_B, \mathbf{x}_S, \omega) r d\theta, \tag{59}$$

where

$$J_1 = \frac{-2}{i\omega\rho} \int_{-\pi/2}^{\pi/2} \partial_i \hat{G}(\mathbf{x}_A, \mathbf{x}_S, \omega) n_i \hat{G}(\mathbf{x}_B, \mathbf{x}_S, \omega) r d\theta \tag{60}$$

and

$$J_2 = \frac{-2}{i\omega\rho} \int_{\pi/2}^{3\pi/2} \partial_i \hat{G}(\mathbf{x}_A, \mathbf{x}_S, \omega) n_i \hat{G}(\mathbf{x}_B, \mathbf{x}_S, \omega) r d\theta. \tag{61}$$

By doing this, only one stationary point of the integrand falls within the domain of integration. So J_2 becomes

$$J_2 = i\omega\rho \frac{e^{-i(k|\mathbf{x}_B| + \frac{\pi}{4})}}{\sqrt{8\pi k|\mathbf{x}_B|}} \tag{62}$$

and equation (59) can be written as

$$\frac{-2}{i\omega\rho} \int_0^{2\pi} \partial_i \hat{G}(\mathbf{x}_A, \mathbf{x}_S, \omega) n_i \hat{G}(\mathbf{x}_B, \mathbf{x}_S, \omega) r d\theta = i\omega\rho \frac{\exp(-i(k|\mathbf{x}_B| + \frac{\pi}{4}))}{\sqrt{8\pi k|\mathbf{x}_B|}} + J_1 \tag{63}$$

with $|\mathbf{x}_B|$ the distance from the origin to $\mathbf{x}_B$, which is the distance between the receivers at $\mathbf{x}_A$ and $\mathbf{x}_B$. The first term on the right-hand side of equation (63) is the impulse response due to a line source at $\mathbf{x}_A$ measured at $\mathbf{x}_B$. Therefore equation (63) is written as

$$\frac{-2}{i\omega\rho} \int_0^{2\pi} \partial_i \hat{G}(\mathbf{x}_A, \mathbf{x}_S, \omega) n_i \hat{G}(\mathbf{x}_B, \mathbf{x}_S, \omega) r d\theta = \hat{G}(\mathbf{x}_B, \mathbf{x}_A, \omega) + J_1. \tag{64}$$

Because the domain contains only one stationary point with contributions from convolutions of inward traveling waves in both states, J_1 may be written as an integral over the entire boundary according to

$$J_1 = \int_0^{2\pi} \frac{-2}{i\omega\rho(\mathbf{x})} (\partial_i \hat{G}_A^{\text{in}}) \hat{G}_B^{\text{in}} n_i r d\theta. \tag{65}$$

Note that there is no contribution from outward traveling waves in both states because the medium is laterally homogeneous. Combining equations (65) and (64) and transforming this back to rectangular coordinates resuls in

$$\hat{G}(\mathbf{x}_A, \mathbf{x}_B, \omega) + \oint_{\partial\mathbb{D}} \frac{-2}{i\omega\rho(\mathbf{x})} \Big((\partial_i \hat{G}_A^{\text{in}}) \hat{G}_B^{\text{in}} + (\partial_i \hat{G}_A^{\text{out}}) \hat{G}_B^{\text{out}} \Big) n_i d^2\mathbf{x} = \oint_{\partial\mathbb{D}} \frac{-2}{i\omega\rho(\mathbf{x})} (\partial_i \hat{G}(\mathbf{x}_A, \mathbf{x}, \omega)) \hat{G}(\mathbf{x}_B, \mathbf{x}, \omega) n_i d^2\mathbf{x}, \tag{66}$$

which again is equation (24). This explicitly shows that equation (24) correctly retrieves the Green's function for a homogeneous fluid medium.

The dipole response $\partial_i \hat{G}(\mathbf{x}_A, \mathbf{x}_S, \omega) n_i$ can be obtained from the monopole response, because receiver A is located at the centre of the circle, $\frac{x_i n_i}{|\mathbf{r}_A|} = -1$. Therefore the dipole response can be obtained by multiplying the monopole response with a factor $-\frac{i\omega}{v}$. This can be seen by comparing equations (40) and (39) (note the extra factor $i\pi/2$ in the argument of the exponential). This indicates that the approximation for the dipole response in equation (25) is valid in this case.

3.2 Numerical examples

A number of numerical models have been conducted to verify equation (29). In all models a different source-receiver configuration is used. The aim of these models is to retrieve the response measured at one receiver due to a virtual source located at the position of the other receiver. This is done using equation (29). The obtained result is then compared to the directly modeled response for an impulsive point source located at

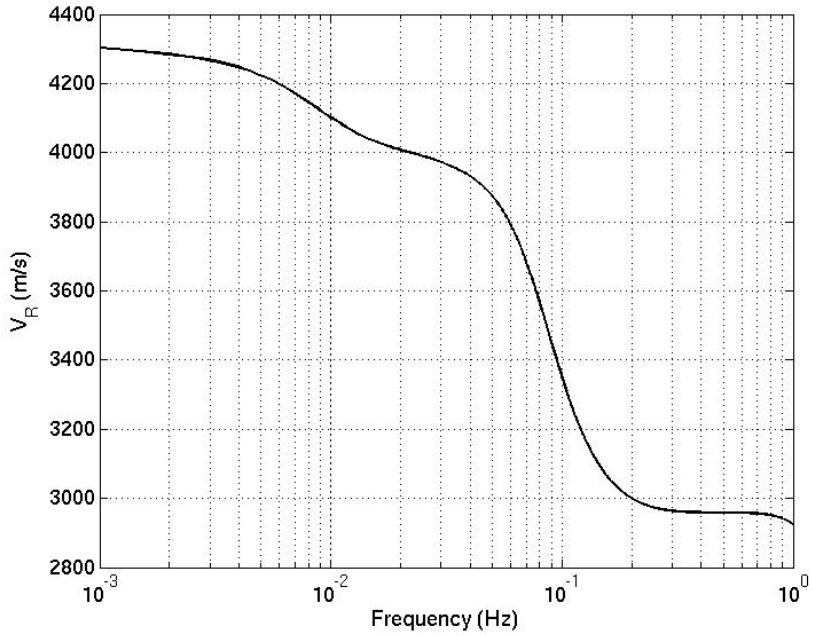

Figure 4: The dispersion curve used in the numerical models. The horizontal axis shows the frequency (ω) and the vertical axis shows the Rayleigh wave velocity (v_R).

one of the receiver locations. It is assumed that the sources only induce fundamental mode Rayleigh waves. Furthermore it is assumed that the Earth is spherically symmetric according to the PREM model (Dziewonski and Anderson, 1981). The dispersion of surface waves has been accounted for, by computing a dispersion curve using the PREM model (figure 4). The impulse responses have been convolved with a source-time function (Ricker wavelet with a peak frequency of 0.1 Hz). For each model, a total of 120 sources is used.

For the first model a circular source distribution has been used (figure 5a). The radius of the circular source distribution is 260 km and the station at $\mathbf{x}_A$ is located at the center of this circle, in the United Kingdom. The station at $\mathbf{x}_B$ is located in the Netherlands, 487.2 km to the east of $\mathbf{x}_A$. The result of this numerical model is shown in figure 6a. In the left part of the figure, the convolutions of the monopole responses measured at the two stations are shown for each source. From the figure it is evident that the system contains two stationary points: one near $\theta = 0°$ and the other near $\theta = 180°$ (figure 3). At these stationary points $|\cos(\alpha_A(\mathbf{x}))| = |\cos(\alpha_B(\mathbf{x}))|$. The red line shown in the stack is the directly modelled reference response. It can be seen that the Green's function is accurately retrieved. For times larger than ~ 250 s new arrivals can be seen in the stack. This part results from the integral on the left-hand side of equation (29). The arrival time of this spurious event corresponds to that of a wave traveling from $\mathbf{x}_A$ to the stationary point on $\partial\mathbb{D}$ at $\theta = 0$ and from there to $\mathbf{x}_B$. The actual Green's function and the result from this left-hand side integral are well separated in time as long as $\mathbf{x}_A$ is not in close proximity to the far end of $\partial\mathbb{D}$ and $\partial\mathbb{D}$ is a sufficiently smooth surface.
Another experiment is done to test how well the two functions are separated in time and to what extent the dipole approximation is valid when $\partial\mathbb{D}$ is not a sphere, but a somewhat irregular surface. In order to do this, the configuration with the constant radius investigated before has been adjusted. The sources are located at a random location between $0.95r$ and $1.05r$ with $r = 260$ km and the sources are all $\Delta\theta = 3°$ apart (figure 5b). The results are shown in figure 6b. For $t < 180$ s the Green's function is still recovered accurately, but at larger times an amplitude error can be seen. The contribution from the left-hand side integral in expression (29) is not as well separated in time for this configuration. This is mainly caused by incomplete destructive interference outside the stationary points. This incomplete interference results in contributions to the convolution stack arriving at times larger than 180 s. Although most of the relevant part of the signal arriving before 180 s is not affected by this and is still accurately recovered. This indicates that the dipole approximation is still valid when $\partial\mathbb{D}$ is a slightly irregular surface and that the left-hand side integral in equation (29) remains separable

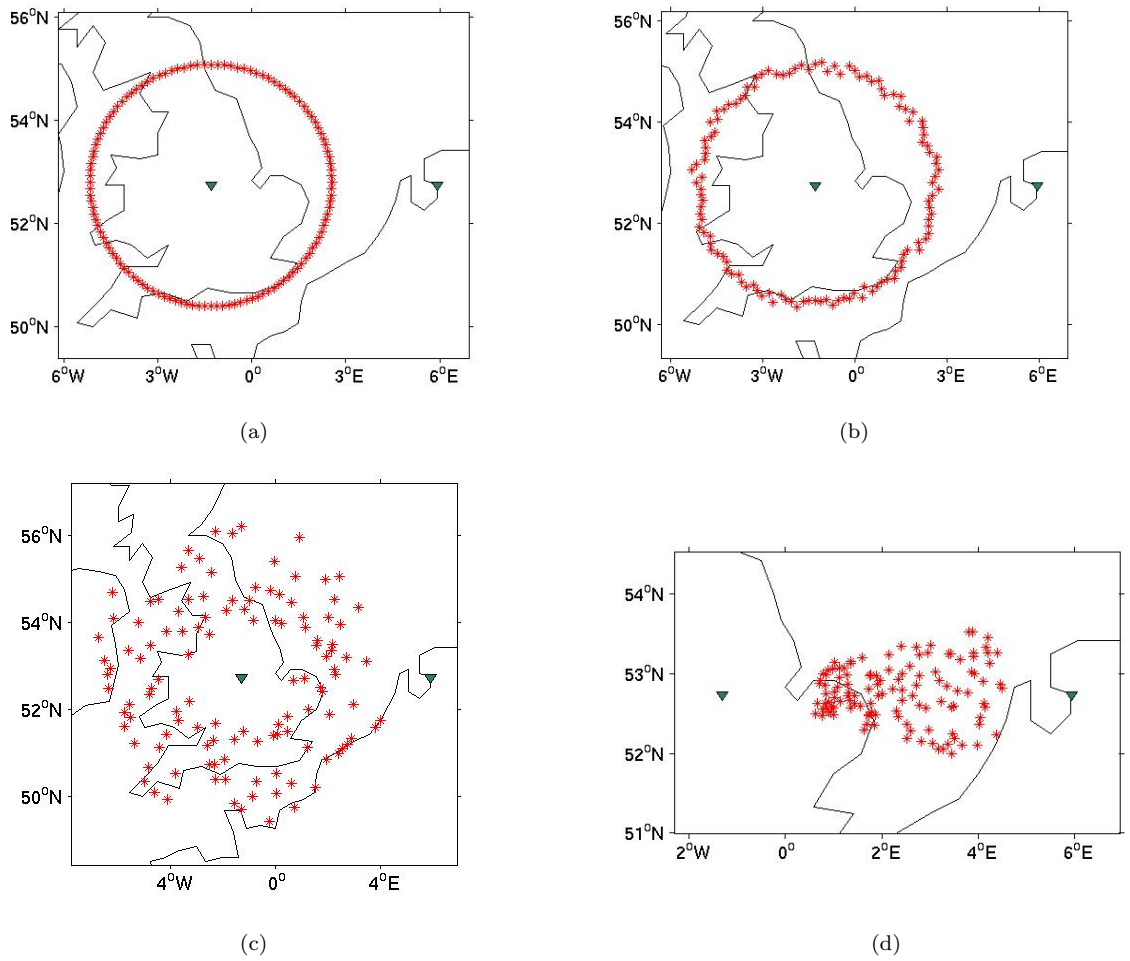

Figure 5: The source-receiver configurations used in the numerical models. The two receivers are located in the United Kingdom ($\mathbf{x}_A$) and in the Netherlands ($\mathbf{x}_B$), respectively. The positions of the source locations in polar coordinates are given by (r_i, θ_i) with the origin located at $\mathbf{x}_A$. The source locations are taken $\Delta\theta$ apart where the distance r_i is varied for each model. (a) $r_i = r = 260$ km for all sources and $\Delta\theta = 3°$. (b) r_i is chosen randomly for each source such that $r_i \in \{0.95r, 1.05r\}$ with $r = 260$ km and $\Delta\theta = 3°$. (c) r_i is chosen randomly for each source such that $r_i \in \{0.5r, 1.5r\}$ with $r = 260$ km and $\Delta\theta = 3°$. (d) r_i is chosen randomly for each source such that $r_i \in \{0.5r, 1.5r\}$ with $r = 260$ km. In this case $\theta_i \in \{73°, 103°\}$ is equidistantly sampled with $\Delta\theta = 0.25°$.

from the relevant signal.

Next, it is investigated if the Green's function is still accurately retrieved when the surface $\partial\mathbb{D}$ is significantly more irregular. In order to do so another numerical model has been run where the sources are located at a random location between $0.5r$ and $1.5r$ with $r = 260$ km and the sources are all $\Delta\theta = 3°$ apart (figure 5c). The result for this model is shown in figure 6c. For $t < 180$ s the Green's function is still recovered accurately, but at larger times an amplitude error can be seen. The last part of the signal is perturbed by the result from incomplete destructive interference for sources located outside of the stationary point. The contributions from sources in the stationary point at $\theta = 0°$ are small compared to the rest of the signal. This indicates that the integral on the left-hand side of equation (29) does not integrate coherently when $\partial\mathbb{D}$ is an sufficiently irregular surface. The approximation for the dipole response used in the derivation of equation (29) is still valid when $\partial\mathbb{D}$ is very irregular, because the relevant part of the signal (before $t = 180$ s) is still recovered accurately.

Finally, it is investigated whether the Green's function can be accurately retrieved when the surface $\partial\mathbb{D}$ is not a closed surface. In order to do so a numerical model is run where all sources are located in the region

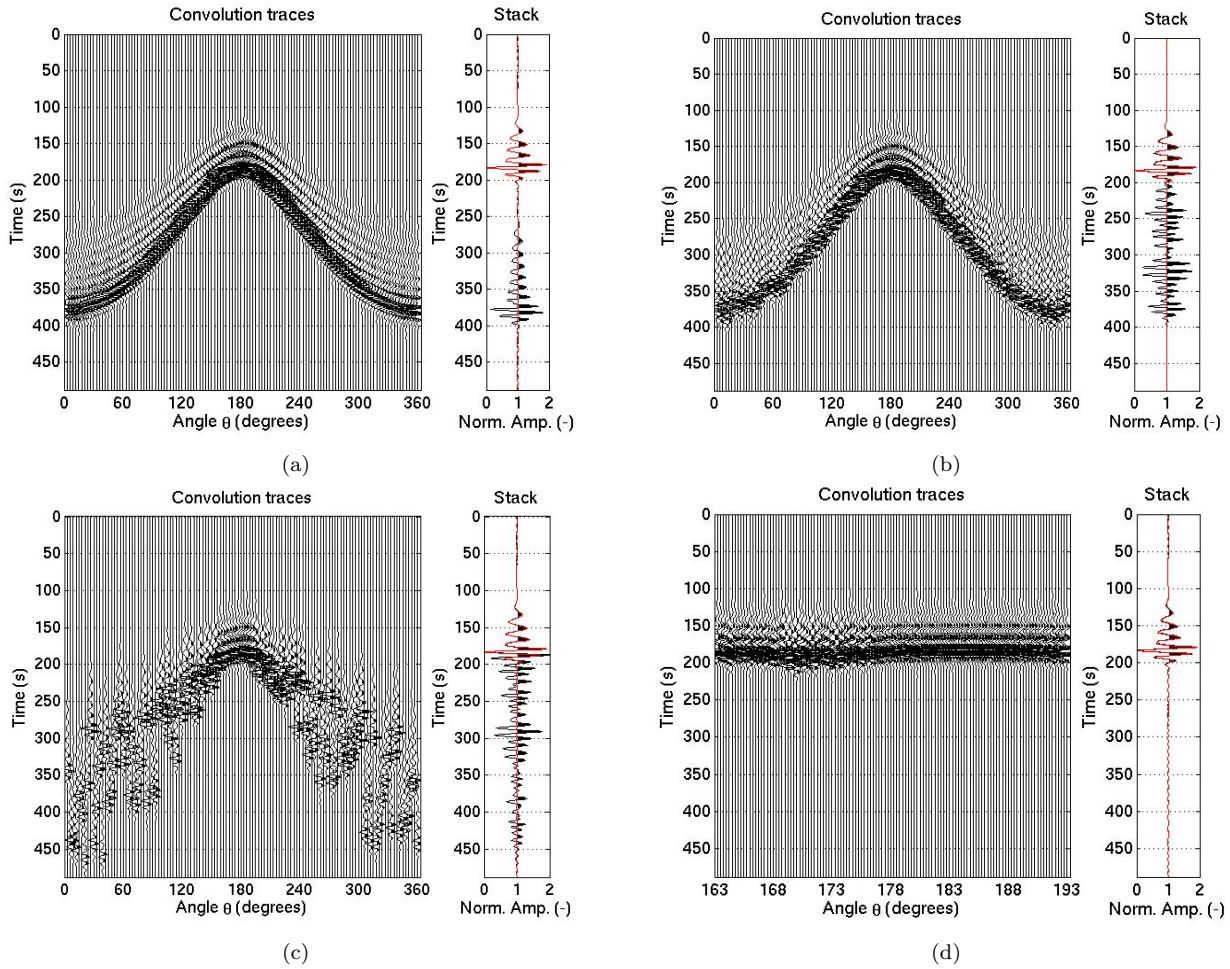

Figure 6: The results obtained for the four different models. The corresponding configurations are shown in figure 5. (a) *Left*: the traces of the convolutions for each source on $\partial\mathbb{D}$ for the configuration shown in figure 5a. Note the stationary points at 0° and 180°. *Right*: the sum of all the traces in the left figure (black) and the reference response (red). Note that the amplitudes are normalized with respect to the largest amplitude in the signal. (b) *Left*: the traces of the convolutions for each source on $\partial\mathbb{D}$ for the configuration shown in figure 5b. Note that the stationary points at $\theta = 0°$ and $\theta = 180°$ are still clearly visible. *Right*: as for (a). (c) *Left*: the traces of the convolutions for each source on $\partial\mathbb{D}$ for the configuration shown in figure 5c. Note that the stationary point at $\theta = 0°$ is still clearly visible whereas the stationary point at $\theta = 180°$ is not. *Right*: as for (a). (d) *Left*: the traces of the convolutions for each source on $\partial\mathbb{D}$ for the configuration shown in figure 5d. In this case, nearly all sources are located in the stationary point. *Right*: as for (a).

between the two receivers (figure 5d). All sources are located between $\theta = 163°$ and $\theta = 193°$. The sources are taken $\Delta\theta = 0.25°$ apart at a random location between $0.5r$ and $1.5r$ where $r = 260$ km is the radius of the circle used in the previous models. A situation in which the source-receiver configuration can be represented by the one in figure 5d would be when one aims to obtain the Green's function between two receivers located on either side of a tectonically active region. The result for this model is shown in figure 6d. In this case all the sources are located close to the stationary point, so only constructive interference occurs. Because of this, no contributions from incomplete interference perturb the signal. This result shows that equation (29) can recover $\hat{G}(\mathbf{x}_A, \mathbf{x}_B, \omega)$ accurately when all sources are located between the two receivers.

4 Interferometry for elastodynamic Green's functions

In this section an expression for elastodynamic Green's functions in arbitrary inhomogeneous, anisotropic solid media is derived. It is then investigated how this expression can be used to retrieve the Green's function from transient source and noise source recordings. A similar approach as in Wapenaar and Fokkema (2006) has been used once more, but starting from a reciprocity theorem of the convolution type instead of a reciprocity theorem of the correlation type.

4.1 Elastodynamic reciprocity theorem

In this section the elastodynamic reciprocity theorem of the convolution type is derived. In any arbitrary, lossless inhomogeneous and anisotropic solid medium the equation of motion in the space-frequency domain is given by

$$i\omega\rho\hat{v}_i - \partial_j\hat{\tau}_{ij} = \hat{f}_i \tag{67}$$

and the stress-strain relation is given by

$$-i\omega s_{ijkl}\hat{\tau}_{kl} + (\partial_j\hat{v}_i + \partial_i\hat{v}_j)/2 = \hat{h}_{ij}, \tag{68}$$

where $\hat{\tau}_{ij}(\mathbf{x},\omega)$ is the stress tensor, $\hat{v}_i(\mathbf{x},\omega)$ is the particle velocity, $\rho(\mathbf{x})$ is the mass density, $s_{ijkl}(\mathbf{x})$ is the compliance, $\hat{f}_i(\mathbf{x},\omega)$ the external volume force density and $\hat{h}_{ij}(\mathbf{x},\omega)$ is the external deformation rate density. Furthermore the interaction quantity is defined as

$$\partial_j\left(\hat{v}_{i,A}\hat{\tau}_{ij,B} - \hat{\tau}_{ij,A}\hat{v}_{i,B}\right). \tag{69}$$

This interaction quantity describes the interaction between two independent elastodynamic states A and B. States A and B are defined by source and medium properties. Consider an arbitrary domain $\mathbb{D}$ with boundary $\partial\mathbb{D}$ and outward pointing normal $\mathbf{n}$. Integration of the interaction quantity over this domain and making use of the divergence theorem, the following equation is obtained:

$$\int_{\mathbb{D}}\partial_j\left(\hat{v}_{i,A}\hat{\tau}_{ij,B} - \hat{\tau}_{ij,A}\hat{v}_{i,B}\right)d^3\mathbf{x} = \oint_{\partial\mathbb{D}}\left(\hat{v}_{i,A}\hat{\tau}_{ij,B} - \hat{\tau}_{ij,A}\hat{v}_{i,B}\right)n_j d^2\mathbf{x}. \tag{70}$$

The integrand in the integral on the left-hand side is expanded using the product rule, resulting in

$$\int_{\mathbb{D}}(\partial_j\hat{v}_{i,A})\hat{\tau}_{ij,B} + \hat{v}_{i,A}\partial_j\hat{\tau}_{ij,B} - (\partial_j\hat{\tau}_{ij,A})\hat{v}_{i,B} - \hat{\tau}_{ij,A}\partial_j\hat{v}_{i,B}d^3\mathbf{x} = \oint_{\partial\mathbb{D}}\left(\hat{v}_{i,A}\hat{\tau}_{ij,B} - \hat{\tau}_{ij,A}\hat{v}_{i,B}\right)n_j d^2\mathbf{x}. \tag{71}$$

The density ρ and the compliance s_{ijkl} are assumed to be equal in both states. Expressions (67) and (68) are used to rewrite equation (71) to

$$\int_{\mathbb{D}} -\hat{\tau}_{ij,A}\hat{h}_{ij,B} - \hat{v}_{i,A}\hat{f}_{i,B} + \hat{h}_{ij,A}\hat{\tau}_{ij,B} + \hat{f}_{i,A}\hat{v}_{i,B}d^3\mathbf{x} = \oint_{\partial\mathbb{D}}\left(\hat{v}_{i,A}\hat{\tau}_{ij,B} - \hat{\tau}_{ij,A}\hat{v}_{i,B}\right)n_j d^2\mathbf{x}. \tag{72}$$

This is the elastodynamic reciprocity theorem of the convolution type (Wapenaar and Fokkema, 2006).

4.2 Interferometry for particle velocity

The sources are chosen as impulsive point sources of force according to

$$\hat{f}_{i,A}(\mathbf{x},\omega) = \delta(\mathbf{x}-\mathbf{x}_A)\delta_{ip} \tag{73}$$

and

$$\hat{f}_{i,B}(\mathbf{x},\omega) = \delta(\mathbf{x}-\mathbf{x}_B)\delta_{iq}. \tag{74}$$

The deformation sources are set equal to zero in both states, so

$$\hat{h}_{ij,A} = 0 \tag{75}$$

and

$$\hat{h}_{ij,B} = 0. \tag{76}$$

In this case $\mathbf{x}_A \in \mathbb{D}$ and $\mathbf{x}_B \notin \mathbb{D}$. The Green's functions are defined to be equal to the particle velocity according to

$$\hat{v}_{i,A}(\mathbf{x},\omega) := \hat{G}^{v,f}_{i,p}(\mathbf{x},\mathbf{x}_A,\omega), \tag{77}$$

and

$$\hat{v}_{i,B}(\mathbf{x},\omega) := \hat{G}^{v,f}_{i,q}(\mathbf{x},\mathbf{x}_B,\omega), \tag{78}$$

The stress tensor is expressed in terms of this Green's function using equation (68) according to

$$\hat{\tau}_{ij,A}(\mathbf{x},\omega) := \hat{G}^{\tau,f}_{ij,p}(\mathbf{x},\mathbf{x}_A,\omega) = (i\omega)^{-1} c_{ijkl}(\mathbf{x})\partial_l \hat{G}^{v,f}_{k,p}(\mathbf{x},\mathbf{x}_A,\omega), \tag{79}$$

and

$$\hat{\tau}_{ij,B}(\mathbf{x},\omega) := \hat{G}^{\tau,f}_{ij,q}(\mathbf{x},\mathbf{x}_B,\omega) = (i\omega)^{-1} c_{ijkl}(\mathbf{x})\partial_l \hat{G}^{v,f}_{k,q}(\mathbf{x},\mathbf{x}_B,\omega). \tag{80}$$

The stiffness matrix c_{ijkl} is the inverse of the compliance and is defined as

$$c_{ijkl}s_{klmn} = s_{ijkl}c_{klmn} = \frac{1}{2}(\delta_{im}\delta_{jn} + \delta_{in}\delta_{jm}). \tag{81}$$

The Green's function $\hat{G}^{v,f}_{i,p}(\mathbf{x},\mathbf{x}_A,\omega)$ represents the i^{th} component of the particle velocity v measured at $\mathbf{x}$ resulting from a unit impulse of force f in the p direction at $\mathbf{x}_A$. Substituting equations (73)-(80) into (72) yields

$$\begin{aligned} &\int_{\mathbb{D}} -\hat{G}^{v,f}_{i,p}(\mathbf{x},\mathbf{x}_A,\omega)\delta(\mathbf{x}-\mathbf{x}_B)\delta_{iq} + \hat{G}^{v,f}_{i,q}(\mathbf{x},\mathbf{x}_B,\omega)\delta(\mathbf{x}-\mathbf{x}_A)\delta_{ip}d^3\mathbf{x} = \\ &\oint_{\partial\mathbb{D}} \Big(\hat{G}^{v,f}_{i,p}(\mathbf{x},\mathbf{x}_A,\omega)\hat{G}^{\tau,f}_{ij,q}(\mathbf{x},\mathbf{x}_B,\omega) - \hat{G}^{\tau,f}_{ij,p}(\mathbf{x},\mathbf{x}_A,\omega)\hat{G}^{v,f}_{i,q}(\mathbf{x},\mathbf{x}_B,\omega)\Big)n_j d^2\mathbf{x}. \end{aligned} \tag{82}$$

Because $\mathbf{x}_B \notin \mathbb{D}$, $\forall\mathbf{x}\ \delta(\mathbf{x}-\mathbf{x}_B) = 0$ on $\partial\mathbb{D}$. Combining this with the shifting property of the delta function, equation (82) becomes

$$\hat{G}^{v,f}_{p,q}(\mathbf{x}_A,\mathbf{x}_B,\omega) = \oint_{\partial\mathbb{D}} \Big(\hat{G}^{v,f}_{i,p}(\mathbf{x},\mathbf{x}_A,\omega)\hat{G}^{\tau,f}_{ij,q}(\mathbf{x},\mathbf{x}_B,\omega) - \hat{G}^{\tau,f}_{ij,p}(\mathbf{x},\mathbf{x}_A,\omega)\hat{G}^{v,f}_{i,q}(\mathbf{x},\mathbf{x}_B,\omega)\Big)n_j d^2\mathbf{x}. \tag{83}$$

Equation (83) is an exact equation for uses in seismic interferometry. It provides the exact Green's function for any lossless inhomogeneous anisotropic solid medium, though the use of this equation is complicated. The integral on the left-hand side of equation (83) contains two convolutions that need to be evaluated. Moreover, all components of the velocity vector and stress tensor must be known for each receiver in both states. The source-receiver reciprocity relations for the particle velocity and stress tensor are defined as $\hat{G}^{v,f}_{q,p}(\mathbf{x}_B,\mathbf{x}_A,\omega) = \hat{G}^{v,f}_{p,q}(\mathbf{x}_A,\mathbf{x}_B,\omega)$ and $\hat{G}^{\tau,f}_{qr,p}(\mathbf{x}_B,\mathbf{x}_A,\omega) = \hat{G}^{v,h}_{p,qr}(\mathbf{x}_A,\mathbf{x}_B,\omega)$ respectively (Wapenaar and Fokkema, 2006). Applying these reciprocity relations to equation (83) results in

$$\hat{G}^{v,f}_{p,q}(\mathbf{x}_A,\mathbf{x}_B,\omega) = \oint_{\partial\mathbb{D}} \Big(\hat{G}^{v,f}_{p,i}(\mathbf{x}_A,\mathbf{x},\omega)\hat{G}^{v,h}_{q,ij}(\mathbf{x}_B,\mathbf{x},\omega) - \hat{G}^{v,h}_{p,ij}(\mathbf{x}_A,\mathbf{x},\omega)\hat{G}^{v,f}_{q,i}(\mathbf{x}_B,\mathbf{x},\omega)\Big)n_j d^2\mathbf{x}. \tag{84}$$

Equation (84) provides the exact impulse response at $\mathbf{x}_A$ due to an impulse of force applied at $\mathbf{x}_B$. However, this expression is still unpractical to use because responses due to both force and deformation sources must be available for each source on $\partial\mathbb{D}$.

4.3 Simplification of the convolution integral

In this section, it is shown that equation (83) can be written in an expression more useful for applications of seismic interferometry. When it is assumed that the medium in a small region near the boundary $\partial\mathbb{D}$ is homogeneous and isotropic, then a Helmholtz decomposition of the velocity field (e.g., Aki and Richards, 2002) can be applied. Doing this, the velocity is written in terms of P- and S-wave potentials $\hat{\phi}$ and $\hat{\psi}_k$ according to

$$\hat{v}_i = -\frac{1}{i\rho\omega}\big(\partial_i\hat{\phi} + \varepsilon_{ijk}\partial_j\hat{\psi}_k\big),\ \partial_l\hat{\psi}_l = 0. \tag{85}$$

For an isotropic and homogeneous medium c_{ijkl} can be written as $c_{ijkl} = \lambda\delta_{ij}\delta_{kl} + \mu(\delta_{ik}\delta_{jl} + \delta_{il}\delta_{jk})$ where the constants λ and μ are the Lamé moduli. Combining this with equation (68) the traction can be written as

$$\tau_{ij}n_j = \frac{1}{i\omega}\big(\lambda(\partial_k\hat{v}_k)n_i + \mu((\partial_j\hat{v}_i)n_j + (\partial_i\hat{v}_j)n_j)\big). \tag{86}$$

Substituting for $\hat{v}_i$ in equation (86) using equation (85) yields

$$\tau_{ij}n_j = \frac{1}{\rho\omega^2}\big(\lambda(\partial_k\partial_k\hat{\phi})n_i + 2\mu(\partial_j\partial_i\hat{\phi})n_j + \mu\partial_j(\varepsilon_{imn}\partial_m\hat{\psi}_n)n_j + \mu\partial_i(\varepsilon_{jmn}\partial_m\hat{\psi}_n)n_j\big). \tag{87}$$

Expanding the products in the right-hand side of equation (72) using expressions (85) and (87) results in several terms containing products of potentials measured at locations $\mathbf{x}_A$ and $\mathbf{x}_B$. To avoid writing all products explicitly, the integrand is written as a superposition of four functions according to

$$\oint_{\partial\mathbb{D}} (\hat{v}_{i,A}\hat{\tau}_{ij,B} - \hat{\tau}_{ij,A}\hat{v}_{i,B})\, n_j d^2\mathbf{x} = -\frac{1}{i\rho^2\omega^3}\oint_{\partial\mathbb{D}} \big(A(\hat{\phi}_A,\hat{\phi}_B) + B(\hat{\phi}_A,\hat{\psi}_{k,B}) + C(\hat{\psi}_{j,A},\hat{\phi}_B) + D(\hat{\psi}_{j,A},\hat{\psi}_{k,B})\big)d^2\mathbf{x}. \tag{88}$$

Each of the terms $A(\hat{\phi}_A,\hat{\phi}_B)$, $B(\hat{\phi}_A,\hat{\psi}_{k,B})$, $C(\hat{\psi}_{j,A},\hat{\phi}_B)$ and $D(\hat{\psi}_{j,A},\hat{\psi}_{k,B})$ is evaluated separately. In order to do this it is assumed that the medium is a sphere where the radius is larger than multiple wavelengths. $\mathbf{x}_A$ is located close to the center of the sphere. In this case, all rays are perpendicular to the surface. Alternatively, an analysis as done by Wapenaar and Fokkema (2006) can be done, where expression (88) is transformed to a local coordinate system for each stationary point. The inner products in equation (88) are then evaluated in this local coordinate system, and transformed back to the original coordinate system. To evaluate the term $A(\hat{\phi}_A,\hat{\phi}_B)$, it is rewritten as

$$A(\hat{\phi}_A,\hat{\phi}_B) = \lambda(\partial_k\partial_k\hat{\phi}_B)(\partial_i\hat{\phi}_A)n_i + 2\mu(\partial_j\partial_i\hat{\phi}_B)(\partial_i\hat{\phi}_A)n_j - \lambda(\partial_k\partial_k\hat{\phi}_A)(\partial_i\hat{\phi}_B)n_i - 2\mu(\partial_j\partial_i\hat{\phi}_A)(\partial_i\hat{\phi}_B)n_j. \tag{89}$$

For high frequencies most of the contributions of $A(\hat{\phi}_A,\hat{\phi}_B)$ to the integral in equation (88) come from a stationary point where the rays are perpendicular to the surface $\partial\mathbb{D}$ or $\cos(\alpha_A) = -\cos(\alpha_B) = -1$. In these stationary points the directional derivatives in equation (89) can be approximated using $(\partial_i\hat{\phi})n_i \approx \pm i\frac{\omega}{v_p}\hat{\phi}$, where the minus sign corresponds to state A and the plus sign to state B. $A(\hat{\phi}_A,\hat{\phi}_B)$ then becomes

$$A(\hat{\phi}_A,\hat{\phi}_B) = -i\frac{\omega}{v_p}\big(\lambda\hat{\phi}_A(\partial_k\partial_k\hat{\phi}_B) + \lambda(\partial_k\partial_k\hat{\phi}_A)\hat{\phi}_B - 4\mu(\partial_i\hat{\phi}_A)(\partial_i\hat{\phi}_B)\big). \tag{90}$$

The P-wave potentials obey the scalar wave equation so that $\partial_k\partial_k\hat{\phi} = -\frac{\omega^2}{v_p^2}\hat{\phi}$. Using the scalar wave equation and the identity $\partial_i\partial_i(\hat{\phi}_A\hat{\phi}_B) = \hat{\phi}_A(\partial_i\partial_i\hat{\phi}_B) + \hat{\phi}_B(\partial_i\partial_i\hat{\phi}_A) + 2(\partial_i\hat{\phi}_A)(\partial_i\hat{\phi}_B)$, equation (90) can be rewritten as

$$A(\hat{\phi}_A,\hat{\phi}_B) = -i\frac{\omega}{v_p}\big((\lambda+2\mu)\hat{\phi}_A(\partial_k\partial_k\hat{\phi}_B) + (\lambda+2\mu)(\partial_k\partial_k\hat{\phi}_A)\hat{\phi}_B - 2\mu\partial_k\partial_k(\hat{\phi}_A\hat{\phi}_B)\big) \tag{91}$$

or

$$A(\hat{\phi}_A,\hat{\phi}_B) = 2i\frac{\omega^3}{v_p^3}(\lambda+2\mu)\hat{\phi}_A\hat{\phi}_B + 2i\frac{\omega}{v_p}\mu\partial_k\partial_k(\hat{\phi}_A\hat{\phi}_B). \tag{92}$$

It is shown in appendix B that $\partial_k\partial_k(\hat{\phi}_A\hat{\phi}_B) = 0$ at the stationary point, therefore

$$A(\hat{\phi}_A, \hat{\phi}_B) = 2i\frac{\rho\omega^3}{v_p}\hat{\phi}_A\hat{\phi}_B \tag{93}$$

or

$$A(\hat{\phi}_A, \hat{\phi}_B) = -2\rho\omega^2(\partial_i\hat{\phi}_A)\hat{\phi}_B. \tag{94}$$

It is shown in appendix D that this result is also valid in more arbitrary domains with different receiver configurations.
The function $B(\hat{\phi}_A, \hat{\psi}_{k,B})$ can be written as

$$B(\hat{\phi}_A, \hat{\psi}_{k,B}) = \mu\partial_i\hat{\phi}_A(\partial_j\varepsilon_{imn}\partial_m\hat{\psi}_{n,B} + \partial_i\varepsilon_{jmn}\partial_m\hat{\psi}_{n,B})n_j - \lambda\partial_k\partial_k\hat{\phi}_A\varepsilon_{imn}\partial_m\hat{\psi}_{n,B}n_i - 2\mu\partial_i\partial_j\hat{\phi}_A\varepsilon_{imn}\partial_m\hat{\psi}_{n,B}n_j \tag{95}$$

The stationary point is located at locations where $\frac{\sin(\alpha_A)}{v_P} = -\frac{\sin(\beta_B)}{v_S}$. For this particular configuration this condition is satisfied when $\sin(\alpha_A) = \sin(\beta_B) = 0$. In the stationary point, the waves to $\mathbf{x}_A$ and $\mathbf{x}_B$ travel perpendicular to the boundary $\partial\mathbb{D}$. This means that the S-wave particle velocity is perpendicular to the normal $\mathbf{n}$. Hence $\varepsilon_{imn}\partial_m\hat{\psi}_{n,B}n_i = 0$. Applying the statements above and the product rule to expression (95) results in

$$\begin{aligned} B(\hat{\phi}_A, \hat{\psi}_{k,B}) =& \mu\partial_j(\partial_i\hat{\phi}_A\varepsilon_{imn}\partial_m\hat{\psi}_{n,B})n_j + \mu\partial_i\hat{\phi}_A\partial_i(\varepsilon_{jmn}\partial_m\hat{\psi}_{n,B}n_j) \\ & - \mu\partial_i\hat{\phi}_A\varepsilon_{jmn}\partial_m\hat{\psi}_{n,B}\partial_i n_j - 3\mu\partial_i\partial_j\hat{\phi}_A\varepsilon_{imn}\partial_m\hat{\psi}_{n,B}n_j. \end{aligned} \tag{96}$$

Because $\partial\mathbb{D}$ is a sphere with a radius larger than several wavelengths, perturbations in the surface $\partial\mathbb{D}$ are small compared to the wavelength of the signal, so that $\partial_i n_j \approx 0$. At this stationary point the P-wave to receiver A travels in opposite direction as the S-wave to receiver B. This means that the particle motions of these waves are perpendicular, or $\partial_i\hat{\phi}_A\varepsilon_{imn}\partial_m\hat{\psi}_{n,B} = 0$ and $\varepsilon_{jmn}\partial_m\hat{\psi}_{n,B}n_j = 0$. Both quantities have an extremum in the stationary point, which implies that their gradients are equal to zero. After rewriting the remaining last term in expression (96) it becomes

$$B(\hat{\phi}_A, \hat{\psi}_{k,B}) = -3\mu\partial_i(\partial_j\hat{\phi}_A\varepsilon_{imn}\partial_m\hat{\psi}_{n,B}n_j) + 3\mu\partial_j\hat{\phi}_A\varepsilon_{imn}\partial_m\hat{\psi}_{n,B}\partial_i n_j + 3\mu\partial_j\hat{\phi}_A\partial_i\varepsilon_{imn}\partial_m\hat{\psi}_{n,B}n_j. \tag{97}$$

Using aforementioned properties, and $\forall g_k\ \partial_i\varepsilon_{ijk}\partial_j g_k = 0$ it can be shown that

$$B(\hat{\phi}_A, \hat{\psi}_{k,B}) = 0. \tag{98}$$

For the term $C(\hat{\psi}_{j,A}, \hat{\phi}_B)$, the derivation is nearly identical as for $B(\hat{\phi}_A, \hat{\psi}_{k,B})$, so

$$C(\hat{\psi}_{j,A}, \hat{\phi}_B) = 0. \tag{99}$$

The results obtained in equations (98) and (99) show that there is no P-wave to S-wave conversion or S-wave to P-wave conversion at the boundary $\partial\mathbb{D}$ for a wave traveling from $\mathbf{x}_B$ to $\mathbf{x}_A$. This is what is to be expected as the boundary $\partial\mathbb{D}$ does not correspond to a physical boundary.
The term $D(\hat{\psi}_{k,A}, \hat{\psi}_{l,B})$ can be written as

$$\begin{aligned} D(\hat{\psi}_{k,A}, \hat{\psi}_{l,B}) =& \mu\big((\partial_j\varepsilon_{imn}\partial_m\hat{\psi}_{n,B})\varepsilon_{ipq}\partial_p\hat{\psi}_{q,A} + (\partial_i\varepsilon_{jmn}\partial_m\hat{\psi}_{n,B})\varepsilon_{ipq}\partial_p\hat{\psi}_{q,A} \\ & - (\partial_j\varepsilon_{ipq}\partial_p\hat{\psi}_{q,A})\varepsilon_{imn}\partial_m\hat{\psi}_{n,B} - (\partial_i\varepsilon_{jpq}\partial_p\hat{\psi}_{q,A})\varepsilon_{imn}\partial_m\hat{\psi}_{n,B}\big)n_j. \end{aligned} \tag{100}$$

The main contributions to the integral from this term come from a stationary point where the rays are parallel but travel in opposite directions. Using again the fact that $(\partial_i f(\mathbf{x}))n_i \approx \pm i\frac{\omega}{v_p}f(\mathbf{x})$ at this stationary point where the minus sign corresponds to state A and the plus sign to state B and that $\forall g_k\ \partial_i\varepsilon_{ijk}\partial_j g_k = 0$, equation (100) becomes

$$\begin{aligned} D(\hat{\psi}_{k,A}, \hat{\psi}_{l,B}) =& \frac{i\omega}{v_s}\mu\big(\varepsilon_{ipq}\partial_p\hat{\psi}_{q,A}\varepsilon_{imn}\partial_m\hat{\psi}_{n,B} + \varepsilon_{ipq}\partial_p\hat{\psi}_{q,A}\varepsilon_{imn}\partial_m\hat{\psi}_{n,B}\big) \\ & + \mu\partial_i\big(\varepsilon_{ipq}\partial_p\hat{\psi}_{q,A}\varepsilon_{jmn}\partial_m\hat{\psi}_{n,B} - \varepsilon_{jpq}\partial_p\hat{\psi}_{q,A}\varepsilon_{imn}\partial_m\hat{\psi}_{n,B}\big)n_j. \end{aligned} \tag{101}$$

Rewriting the last two terms using the product rule, equation (101) can be rewritten as

$$D(\hat{\psi}_{k,A},\hat{\psi}_{l,B}) = \frac{2i\omega\mu}{v_s}\varepsilon_{ipq}\varepsilon_{imn}\partial_p\hat{\psi}_{q,A}\partial_m\hat{\psi}_{n,B} + \mu\partial_i\big(\big(\varepsilon_{ipq}\partial_p\hat{\psi}_{q,A}\varepsilon_{jmn}\partial_m\hat{\psi}_{n,B} - \varepsilon_{jpq}\partial_p\hat{\psi}_{q,A}\varepsilon_{imn}\partial_m\hat{\psi}_{n,B}\big)n_j\big) - \mu\big(\varepsilon_{ipq}\partial_p\hat{\psi}_{q,A}\varepsilon_{jmn}\partial_m\hat{\psi}_{n,B} - \varepsilon_{jpq}\partial_p\hat{\psi}_{q,A}\varepsilon_{imn}\partial_m\hat{\psi}_{n,B}\big)\partial_i n_j. \tag{102}$$

The product of two Levi-Civita symbols is written as $\varepsilon_{ipq}\varepsilon_{imn} = \delta_{pm}\delta_{qn} - \delta_{pn}\delta_{qm}$. At the stationary point the particle motions described by $\varepsilon_{jpq}\partial_p\hat{\psi}_{q,A}$ and $\varepsilon_{jmn}\partial_m\hat{\psi}_{n,B}$ are perpendicular to n_j. Therefore the inner products $\varepsilon_{jpq}\partial_p\hat{\psi}_{q,A}n_j$ and $\varepsilon_{jmn}\partial_m\hat{\psi}_{n,B}n_j$ in equation (102) vanish. Using this and the fact that $\partial_i n_j \approx 0$, equation (102) is reduced to

$$D(\hat{\psi}_{k,A},\hat{\psi}_{l,B}) = \frac{2i\omega\mu}{v_s}\big(\partial_m\hat{\psi}_{n,A}\partial_m\hat{\psi}_{n,B} - \partial_n\hat{\psi}_{m,A}\partial_m\hat{\psi}_{n,B}\big). \tag{103}$$

Using the product rule twice and the fact that $\partial_n\hat{\psi}_n = 0$, equation (103) becomes

$$D(\hat{\psi}_{k,A},\hat{\psi}_{l,B}) = \frac{i\omega\mu}{v_s}\big(\partial_m\partial_m(\hat{\psi}_{n,A}\hat{\psi}_{n,B}) - \hat{\psi}_{n,A}\partial_m\partial_m\hat{\psi}_{n,B} - \hat{\psi}_{n,B}\partial_m\partial_m\hat{\psi}_{n,A} - 2\partial_n(\hat{\psi}_{m,A}\partial_m\hat{\psi}_{n,B})\big). \tag{104}$$

At the stationary point $\partial_m\partial_m(\hat{\psi}_{n,A}\hat{\psi}_{n,B}) = 0$ and $\partial_n(\hat{\psi}_{m,A}\partial_m\hat{\psi}_{n,B}) = 0$ (Appendix B). Combining these results with the vector wave equation $\partial_m\partial_m\hat{\psi}_n = -\frac{\omega^2}{v_s^2}\hat{\psi}_n$ results in

$$D(\hat{\psi}_{k,A},\hat{\psi}_{l,B}) = 2i\frac{\omega^3}{v_s^3}\mu\hat{\psi}_{n,A}\hat{\psi}_{n,B}. \tag{105}$$

Substitution of the approximation for the dipole, $\big(\partial_i f(\mathbf{x})\big)n_i \approx \pm i\frac{\omega}{v_p}f(\mathbf{x})$, results in

$$D(\hat{\psi}_{k,A},\hat{\psi}_{l,B}) = -2\omega^2\rho(\partial_i\hat{\psi}_{n,A})\hat{\psi}_{n,B}n_i. \tag{106}$$

Upon substitution of equations (94), (98), (99), and (106), equation (88) becomes

$$\oint_{\partial\mathbb{D}}\left(\hat{v}_{i,A}\hat{\tau}_{ij,B} - \hat{\tau}_{ij,A}\hat{v}_{i,B}\right)n_j d^2\mathbf{x} = \frac{2}{i\rho\omega}\oint_{\partial\mathbb{D}}\big((\partial_i\hat{\phi}_A)\hat{\phi}_B + (\partial_i\hat{\psi}_{n,A})\hat{\psi}_{n,B}\big)n_i d^2\mathbf{x}. \tag{107}$$

Note the similarities between this result and the result obtained for elastodynamic Green's function representations using cross-correlations shown in equation (A-8) in Wapenaar and Fokkema (2006). In order to obtain a Green's function representation for use in interferometry, the P- and S-wave potentials must be expressed in terms of Green's functions. In order to do this, the same approach as Wapenaar and Fokkema (2006) is used. Wapenaar and Fokkema (2006) express the measured P- and S-wave potentials at $\mathbf{x}$ due to a unit impulse of force at $\mathbf{x}_A$ as

$$\hat{\phi}_A(\mathbf{x},\omega) := \hat{G}^{\phi,f}_{0,p}(\mathbf{x},\mathbf{x}_A,\omega) \tag{108}$$

and

$$\hat{\psi}_{k,A}(\mathbf{x},\omega) := \hat{G}^{\psi,f}_{k,p}(\mathbf{x},\mathbf{x}_A,\omega). \tag{109}$$

Similar expressions hold for a source at $\mathbf{x}_B$. The Green's functions given above can be combined into one Green's function $\hat{G}^{P,f}_{K,p}(\mathbf{x},\mathbf{x}_A,\omega)$ where $P = \phi$ when $K = 0$ or $P = \psi_k$ when $K = k$, $k \in \{1,2,3\}$. Applying the newly defined Green's function to equation (107) and combining it with equation (83) results in

$$\hat{G}^{v,f}_{p,q}(\mathbf{x}_A,\mathbf{x}_B,\omega) = \frac{2}{i\rho\omega}\oint_{\partial\mathbb{D}}(\partial_i\hat{G}^{P,f}_{K,p}(\mathbf{x},\mathbf{x}_A,\omega)\hat{G}^{P,f}_{K,q}(\mathbf{x},\mathbf{x}_B,\omega)n_i d^2\mathbf{x}. \tag{110}$$

Substituting the source-receiver reciprocity relations

$$\hat{G}^{P,f}_{K,p}(\mathbf{x},\mathbf{x}_A,\omega) = \hat{G}^{v,P}_{p,K}(\mathbf{x}_A,\mathbf{x},\omega) \tag{111}$$

and

$$\hat{G}^{P,f}_{K,q}(\mathbf{x},\mathbf{x}_B,\omega) = \hat{G}^{v,P}_{q,K}(\mathbf{x}_B,\mathbf{x},\omega) \tag{112}$$

into equation (110) results in

$$\hat{G}^{v,f}_{p,q}(\mathbf{x}_A,\mathbf{x}_B,\omega) = \frac{2}{i\rho\omega}\oint_{\partial\mathbb{D}} (\partial_i \hat{G}^{v,P}_{p,K}(\mathbf{x}_A,\mathbf{x},\omega))\hat{G}^{v,P}_{q,K}(\mathbf{x}_B,\mathbf{x},\omega)n_i d^2\mathbf{x}. \tag{113}$$

When $\partial\mathbb{D}$ is a sphere with a large radius, the dipole response can again be approximated using

$$\partial_i \hat{G}^{v,P}_{p,K}(\mathbf{x}_A,\mathbf{x},\omega)n_i = -\frac{i\omega}{v_K}\hat{G}^{v,P}_{p,K}(\mathbf{x}_A,\mathbf{x},\omega) \tag{114}$$

where $v_K = v_p$ for $K = 0$ or $v_K = v_s$ for $K \in \{1,2,3\}$. Note that there is no summation over index K in this equation. Using this approximation in equation (113) yields

$$\hat{G}^{v,f}_{p,q}(\mathbf{x}_A,\mathbf{x}_B,\omega) = -\frac{2}{\rho v_K}\oint_{\partial\mathbb{D}} \hat{G}^{v,P}_{p,K}(\mathbf{x}_A,\mathbf{x},\omega)\hat{G}^{v,P}_{q,K}(\mathbf{x}_B,\mathbf{x},\omega)d^2\mathbf{x}. \tag{115}$$

Equation (115) is more practical to use than equation (84). Equation (115) states that the particle velocity at $\mathbf{x}_A$ that would result from a impulsive point source at $\mathbf{x}_B$ can be obtained from the responses measured by the two receivers. In order to do so, the particle velocity responses resulting from P- and S-wave sources are required. The responses at both stations have to be cross-convolved and the results have to be stacked over all source locations.

4.4 Transient sources

The result obtained in the previous section is only valid when the sources are impulsive point sources of force (Equations (73) and (74)). When this method is applied to real data, the sources are no impulsive point sources but transient sources which generate a wavelet $s^K(\mathbf{x},t)$ (Wapenaar and Fokkema, 2006). In this subsection a new expression is derived for equation (115) so that it can be applied to real data. The observed quantity, in this case the particle velocity, at the receivers at $\mathbf{x}_A$ and $\mathbf{x}_B$ is the Green's function convolved with the source wavelet. In the frequency domain this is expressed as

$$\hat{v}^{\text{obs}}_{p,K}(\mathbf{x}_A,\mathbf{x},\omega) = \hat{G}^{v,P}_{p,K}(\mathbf{x}_A,\mathbf{x},\omega)\hat{s}^K(\mathbf{x},\omega) \tag{116}$$

for the station at $\mathbf{x}_A$ and

$$\hat{v}^{\text{obs}}_{q,K}(\mathbf{x}_B,\mathbf{x},\omega) = \hat{G}^{v,P}_{q,K}(\mathbf{x}_B,\mathbf{x},\omega)\hat{s}^K(\mathbf{x},\omega) \tag{117}$$

for the station at $\mathbf{x}_B$, where $\hat{s}^K(\mathbf{x},\omega)$ is the spectrum of the wavelet for different potentials ($K \in \{0,1,2,3\}$). When this is applied to equation (115) the following expression is obtained:

$$\hat{G}^{v,f}_{p,q}(\mathbf{x}_A,\mathbf{x}_B,\omega) = -\frac{2}{\rho v_K}\oint_{\partial\mathbb{D}} \frac{1}{\hat{S}^K}\hat{v}^{\text{obs}}_{p,K}(\mathbf{x}_A,\mathbf{x},\omega)\hat{v}^{\text{obs}}_{q,K}(\mathbf{x}_B,\mathbf{x},\omega)d^2\mathbf{x}, \tag{118}$$

where $\hat{S}^K(\mathbf{x},\omega)$ is the autoconvolution of the source wavelet. The spectrum of the source wavelet can be split in an amplitude spectrum and a phase spectrum according to $\hat{s}^K(\mathbf{x},\omega) = \hat{A}^K(\mathbf{x},\omega)e^{i\hat{\Phi}^K(\mathbf{x},\omega)}$. Note that the phase of the spectrum is a function of the source activation time. The autoconvolution and autocorrelation of the source wavelet are defined by $\hat{S}^K(\mathbf{x},\omega) := (\hat{s}^K(\mathbf{x},\omega))^2 = (\hat{A}^K(\mathbf{x},\omega))^2 e^{2i\hat{\Phi}^K(\mathbf{x},\omega)}$ and $\hat{R}^K(\mathbf{x},\omega) := \hat{s}^K(\mathbf{x},\omega)(\hat{s}^K(\mathbf{x},\omega))^* = (\hat{A}^K(\mathbf{x},\omega))^2$, respectively. Unlike for the autocorrelation, the phase of the source wavelet is not eliminated in the autoconvolution. Therefore, in order to evaluate the integral in equation (118) the amplitude spectrum and the phase spectrum must be known for each source on $\partial\mathbb{D}$. The largest contributions to the integral in equation (118) come from near the stationary points on $\partial\mathbb{D}$. Therefore it is only necessary that $\hat{S}^K(\mathbf{x},\omega)$ is known accurately for sources near the stationary point.

4.5 Noise sources

When uncorrelated noise sources are used instead of transient sources, the same problem as for the acoustic interferometry arises when using this method. This problem is again explained using a similar analysis as Wapenaar and Fokkema (2006). Suppose $\partial\mathbb{D}$ consists of a large amount of simultaneously acting P- and S-wave noise sources with identical power spectra. The spectrum of the noise source is given by $\hat{N}_K(\mathbf{x},\omega)$ where subscript $K \in \{0,1,2,3\}$ defines the type of noise source. When all noise sources act simultaneously, the observed particle velocities at $\mathbf{x}_A$ and $\mathbf{x}_B$ are given by

$$\hat{v}_p^{\mathrm{obs}}(\mathbf{x}_A,\omega) = \oint_{\partial\mathbb{D}} \hat{G}^{v,P}_{p,K}(\mathbf{x}_A,\mathbf{x},\omega)\hat{N}_K(\mathbf{x},\omega)d^2\mathbf{x} \tag{119}$$

and

$$\hat{v}_q^{\mathrm{obs}}(\mathbf{x}_B,\omega) = \oint_{\partial\mathbb{D}} \hat{G}^{v,P}_{q,L}(\mathbf{x}_B,\mathbf{x}',\omega)\hat{N}_L(\mathbf{x}',\omega)d^2\mathbf{x}', \tag{120}$$

respectively. Using the same reasoning as before it can be shown that the spectra of two uncorrelated noise sources $\hat{N}_K(\mathbf{x},\omega)$ and $\hat{N}_L(\mathbf{x}',\omega)$ follow the relation

$$\langle \hat{N}_K(\mathbf{x},\omega)\hat{N}_L(\mathbf{x}',\omega)\rangle = 0. \tag{121}$$

$\langle\cdot\rangle$ represents spatial ensemble averaging, which is usually replaced by measuring the signals over a large time interval and taking the average (e.g., Wapenaar et al., 2011 and Slob et al., 2007). When the spatial ensemble average over source locations of the observed acoustic particle velocity is taken and combined with equation (121) the following relation is obtained

$$\langle \hat{v}^{\mathrm{obs}}_{p,K}(\mathbf{x}_A,\omega)\hat{v}^{\mathrm{obs}}_{q,K}(\mathbf{x}_B,\omega)\rangle = 0. \tag{122}$$

This result shows that the velocity measurements resulting from simultaneously active uncorrelated noise sources can not be used to obtain the Green's function between the two receivers using interferometry by convolution. In deriving this expression, it is assumed that the noise sources act at the same time, which is not always the case. For some noise sources it is a better assumption that the sources are active in succession (e.g., microseisms). The dominating source will be at a different location each day, depending on the weather conditions. In this case the Green's function can be retrieved using expression (118). The source time functions for these kinds of noise sources are long and generally unknown, hence the correction for the autoconvolution cannot be made properly. In either case, the Green's function cannot be retrieved using the autoconvolution of seismic noise recordings.

5 Conclusions

In this work, exact expressions for Green's functions in lossless fluid and solid media have been derived from reciprocity theorems. The convolutions of observed wavefields at two observation points have been integrated over source positions to retrieve the Green's function between these observation points. No assumptions have been made about the homogeneity or isotropy of the media. The observed wavefields have been generated by an arbitrary distribution of sources. It is necessary that one of the observation points is enclosed by this source distribution whereas the other is not.

In their exact form the obtained expressions are not efficient for use in seismic interferometry. The exact form of the expressions contains two convolution products that must be computed for each source. Furthermore, in the acoustic case, the acoustic pressure responses from both monopole and dipole sources must be available for all source locations. In the elastodynamic case the particle velocity responses due to both force and deformation sources must be known for each source. The main contributions to these integrals result from stationary points in the source region. When the source region is sufficiently smooth, the integral expression can be simplified. In the acoustic case the simplified integrand contains only one convolution product and the responses of dipole sources are no longer required. For solid media, the new Green's function representation also contains one convolution product and only responses from monopole P- and S-wave sources are required.

The derived expressions are only valid when the sources are impulsive point sources. In order to make these expressions usable for Green's function retrieval using data from transient sources, a correction for the source

wavelet has to be made. In order to do so, the autocorrelation and the exact source activation time have to be known. Seismic interferometry is often done using the data recorded from uncorrelated noise sources. For noise sources, the source-time functions are generally unknown and hence the correction for the source wavelet cannot be made, implying that the responses from noise sources cannot be used in seismic interferometry by cross-convolution.

Acknowledgements

I would like to thank Elmer Ruigrok for providing me with an initial version of the code that was used in this work, for our insightful discussions and most of all for his great supervision. Hanneke Paulssen proved to be one of the best second supervisors, because of her valuable help during my entire thesis and especially during the start up phase of the project. Kees Wapenaar has provided excellent help with some problems I encountered during my work. My roommates in the 'seismology student room', Maurits Metman, Robert Warmer and Iris van Zelst, ensured that the whole project was a very pleasant experience and on top of that they revised various versions of this work.

Appendix

A Numerical verification of equation (18)

In this section a numerical example is given to illustrate the validity of equation (18). In this example, a circular source configuration is used (figure 7). The sources are numbered, starting from 1 at the northernmost source, counting clockwise. The radius of this circle is 260 km and the receiver at location $\mathbf{x}_A$ is located at the center of this circle. $\mathbf{x}_A$ is located in the United Kingdom and $\mathbf{x}_B$ is located in the Netherlands. A total of 120 sources are used. The responses measured at both receivers are directly modelled for each source on $\partial\mathbb{D}$. The response $\hat{G}(\mathbf{x}_A, \mathbf{x}_B, \omega)$ is obtained from these responses. The computed result is then compared to the directly modelled response for a impulsive point source located at one of the receiver locations. It is assumed that the sources only induce fundamental mode Rayleigh waves. Furthermore it is assumed that the Earth is spherically symmetric according to the PREM model (Dziewonski and Anderson, 1981). The dispersion of surface waves has been accounted for, by computing a dispersion curve using the PREM model (figure 4). The impulse responses have been convolved with a source-time function (Ricker wavelet with a peak frequency of 0.1 Hz). Equation (18) is repeated here for easier reference

$$\begin{aligned}\hat{G}(\mathbf{x}_A, \mathbf{x}_B, \omega) = \oint_{\partial\mathbb{D}} \frac{1}{i\omega\rho(\mathbf{x})} \Big(&\hat{G}(\mathbf{x}_A, \mathbf{x}, \omega)\partial_i \hat{G}(\mathbf{x}_B, \mathbf{x}, \omega) \\ &- (\partial_i \hat{G}(\mathbf{x}_A, \mathbf{x}, \omega))\hat{G}(\mathbf{x}_B, \mathbf{x}, \omega)\Big) n_i d^2\mathbf{x}.\end{aligned} \tag{123}$$

The responses $\hat{G}(\mathbf{x}_A, \mathbf{x}, \omega)$, $\partial_i \hat{G}(\mathbf{x}_A, \mathbf{x}, \omega)n_i$, $\hat{G}(\mathbf{x}_B, \mathbf{x}, \omega)$, $\partial_i \hat{G}(\mathbf{x}_B, \mathbf{x}, \omega)n_i$, are shown in figures 8a, 8c, 8b and 8d, respectively. The first term of the integrand in equation (123) consists of the convolution of $\hat{G}(\mathbf{x}_A, \mathbf{x}, \omega)$ with $\partial_i \hat{G}(\mathbf{x}_B, \mathbf{x}, \omega)n_i$. The evaluation of this term for each source and the sum of these responses are shown in figure 9a. Note that the amplitude has been scaled with respect to the largest amplitude in the signal. Two distinct signals can be seen, the first arriving at $t = 130$ s and the second arriving at $t = 270$ s. The first of these signals corresponds to the reference response. The second term of the integrand in equation (123) consists of the convolution of $\partial_i \hat{G}(\mathbf{x}_A, \mathbf{x}, \omega)n_i$ with $\hat{G}(\mathbf{x}_B, \mathbf{x}, \omega)$. The evaluation of this term for each source and the sum of these responses are shown in figure 9b. Note that the amplitude has again been scaled with respect to the largest amplitude in the signal. Two distinct signals can be seen, the first arriving at $t = 130$ s and the second arriving at $t = 270$ s. The first of these signals corresponds to the reference response, but of reversed polarity. Next, the difference of these two terms is taken. This result is shown in figure 9c. It is seen that by taking the difference the first arrival now matches the reference response exactly whereas the contribution from the second signal has canceled. This result shows that $\hat{G}(\mathbf{x}_A, \mathbf{x}_B, \omega)$ is accurately retrieved using equation (18).

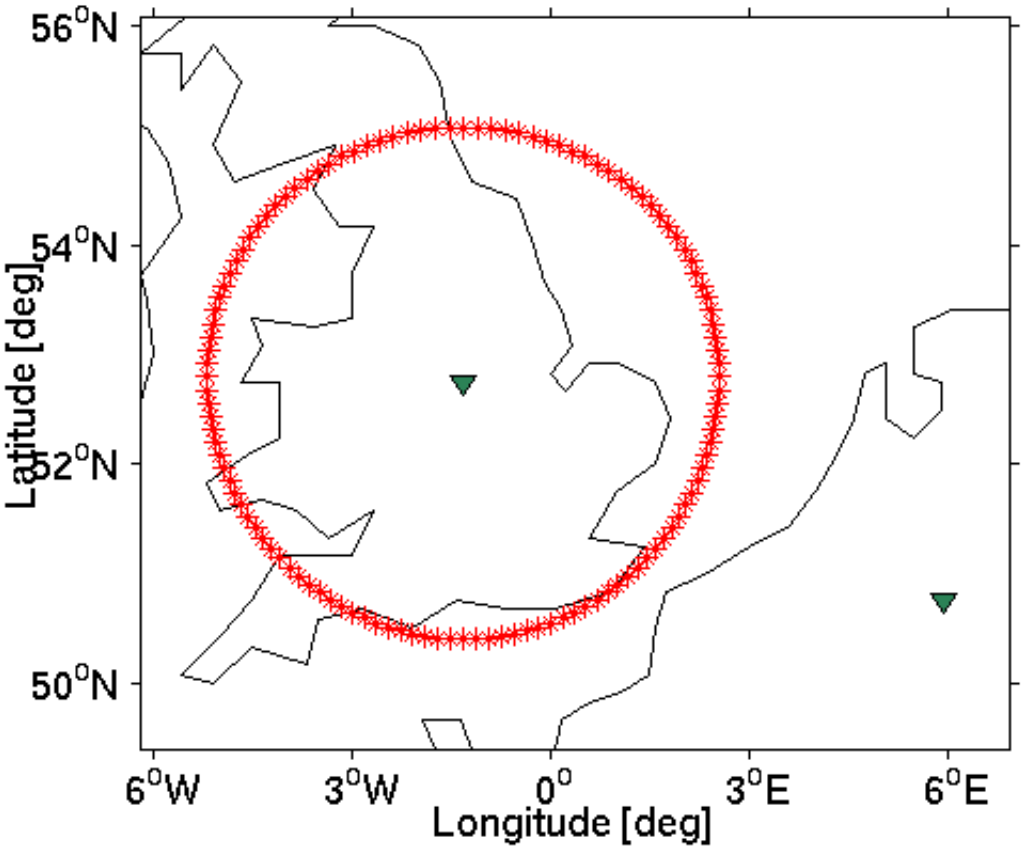

Figure 7: The source-receiver configuration used in the numerical example. The two receivers are located in the United Kingdom and in the Netherlands, respectively.

B Evaluation of expressions in the stationary point

In this section it is shown that several expressions are equal to zero in the stationary point. Consider the quantity $\partial_i \partial_i (\hat{\phi}_A \hat{\phi}_B)$. It is integrated over the arbitrary domain $\mathbb{D}$ with boundary $\partial\mathbb{D}$. Application of the divergence theorem results in

$$\int_{\mathbb{D}} \partial_i \partial_i (\hat{\phi}_A \hat{\phi}_B) d^3\mathbf{x} = \int_{\partial\mathbb{D}} \partial_i (\hat{\phi}_A \hat{\phi}_B) n_i d^2\mathbf{x}. \tag{124}$$

Using the product rule this becomes

$$\int_{\mathbb{D}} \partial_i \partial_i (\hat{\phi}_A \hat{\phi}_B) d^3\mathbf{x} = \int_{\partial\mathbb{D}} \hat{\phi}_A (\partial_i \hat{\phi}_B) n_i + \hat{\phi}_B (\partial_i \hat{\phi}_A) n_i d^2\mathbf{x}. \tag{125}$$

Applying $\partial_i f(\mathbf{x}) n_i \approx -i\frac{\omega}{v_p}\cos(\alpha) f(\mathbf{x})$ yields

$$\int_{\mathbb{D}} \partial_i \partial_i (\hat{\phi}_A \hat{\phi}_B) d^3\mathbf{x} = -\frac{i\omega}{v_p} \int_{\partial\mathbb{D}} \hat{\phi}_A \hat{\phi}_B \cos(\alpha_B) + \hat{\phi}_A \hat{\phi}_B \cos(\alpha_A) d^2\mathbf{x}. \tag{126}$$

Because the stationary point is located where $\cos(\alpha_A) = -\cos(\alpha_B)$ it follows that

$$\int_{\mathbb{D}} \partial_i \partial_i (\hat{\phi}_A \hat{\phi}_B) d^3\mathbf{x} = 0, \tag{127}$$

therefore it can be concluded that $\partial_i \partial_i (\hat{\phi}_A \hat{\phi}_B) = 0$ at the stationary point.

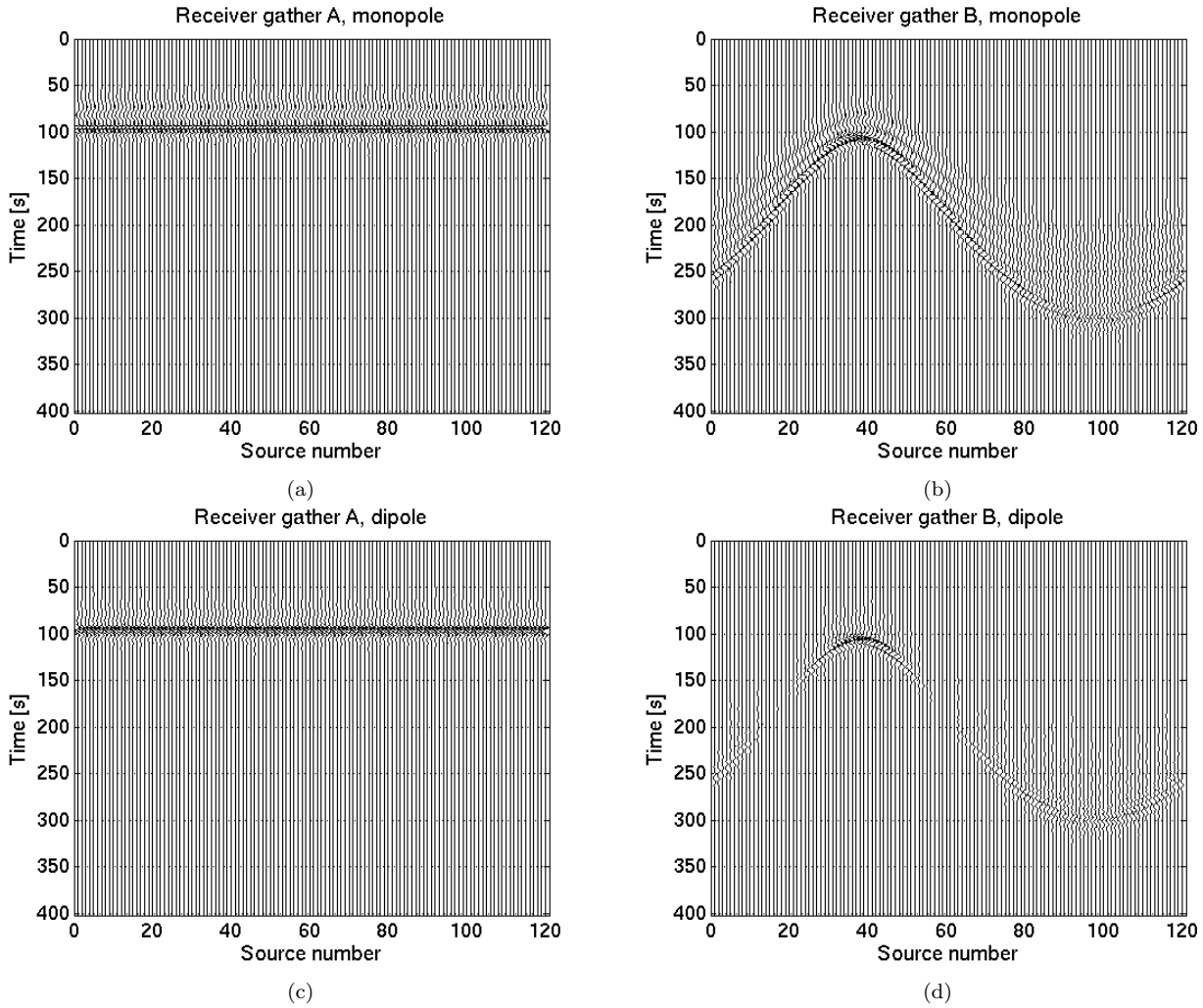

Figure 8: The directly modelled responses. (a) Monopole response as observed by receiver A. (b) Monopole response as observed by receiver B. (c) Dipole response as observed by receiver A. (d) Dipole response as observed by receiver B.

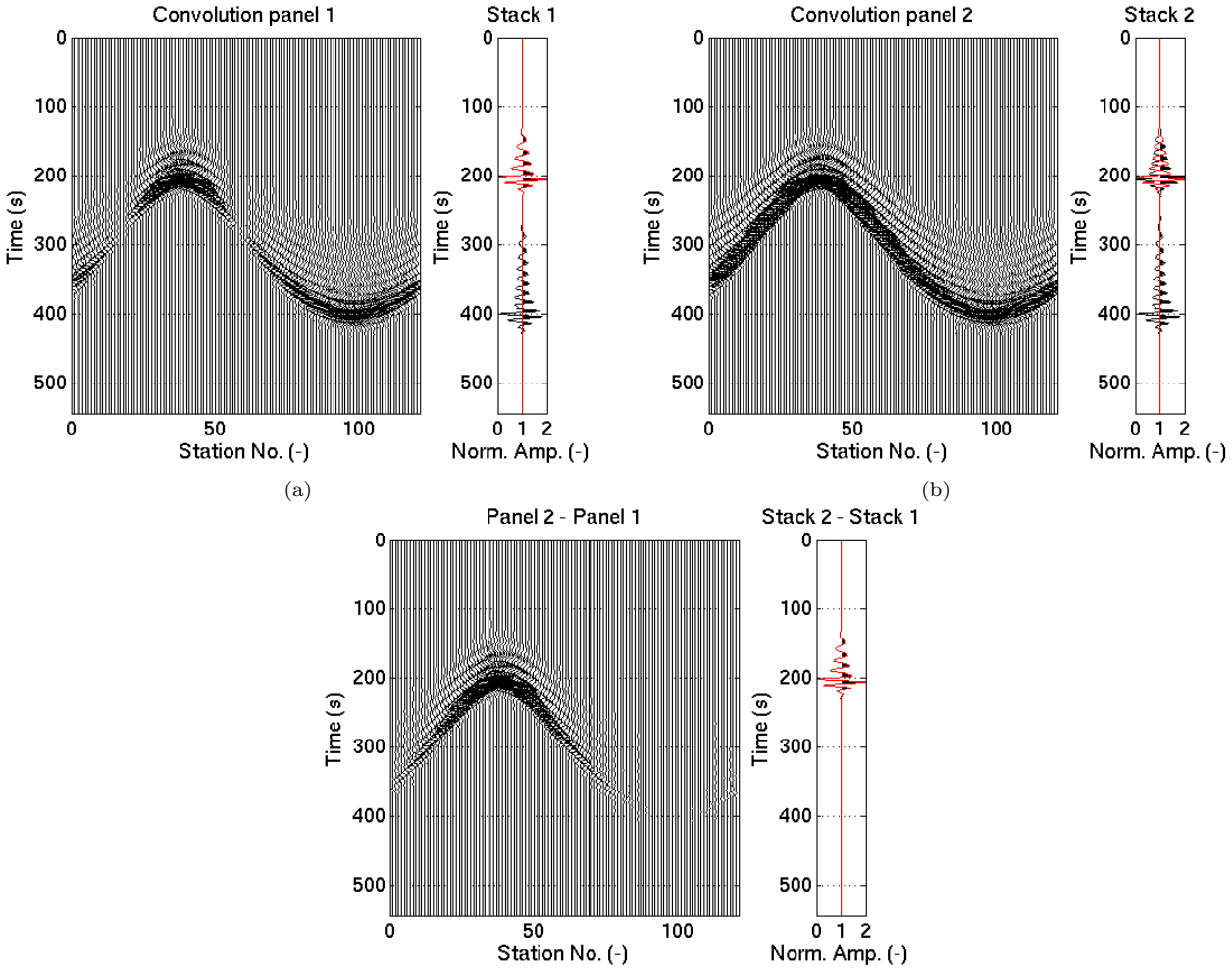

Figure 9: (a) *Left*: the traces of the convolutions from the first term in equation (123) for each source on $\partial\mathbb{D}$. These are the convolutions of the responses shown in figures 8a and 8d. *Right*: the sum of all the traces in the left figure (black) and the reference response (red). Note that the amplitudes are normalized with respect to the largest amplitude in the signal. (b) *Left*: the traces of the convolutions from the second term in equation (123) for each source on $\partial\mathbb{D}$. These are the convolutions of the responses shown in figures 8b and 8c. *Right*: as for (a). (c) *Left*: the traces of the difference between the convolutions shown in figures 9a and 9b. *Right*: as for (a).

Next, consider the quantity $\partial_n(\hat{\psi}_{m,A}\partial_m\hat{\psi}_{n,B})$. It is integrated over the domain $\mathbb{D}$ with boundary $\partial\mathbb{D}$. Application of the divergence theorem results in

$$\int_{\mathbb{D}} \partial_n(\hat{\psi}_{m,A}\partial_m\hat{\psi}_{n,B})d^3\mathbf{x} = \int_{\partial\mathbb{D}} (\hat{\psi}_{m,A}\partial_m\hat{\psi}_{n,B})n_n d^2\mathbf{x}. \tag{128}$$

Because $\partial\mathbb{D}$ is a sphere with a large radius $\partial_m n_n = 0$. Therefore it is evident that

$$\int_{\mathbb{D}} \partial_n(\hat{\psi}_{m,A}\partial_m\hat{\psi}_{n,B})d^3\mathbf{x} = \int_{\partial\mathbb{D}} (\hat{\psi}_{m,A}\partial_m(\hat{\psi}_{n,B}n_n))d^2\mathbf{x}. \tag{129}$$

$\hat{\psi}_{n,B}$ describes the direction of wave propagation, and is therefore parallel to n_n at the boundary in the stationary point. This implies that $\hat{\psi}_{n,B}n_n$ has an extremum at the stationary point, so that $\partial_m(\hat{\psi}_{n,B}n_n) = 0$. Substituting this result in the right-hand side integral in expression (129) yields

$$\int_{\mathbb{D}} \partial_n(\hat{\psi}_{m,A}\partial_m\hat{\psi}_{n,B})d^3\mathbf{x} = 0. \tag{130}$$

Therefore it can be concluded that $\partial_n(\hat{\psi}_{m,A}\partial_m\hat{\psi}_{n,B}) = 0$ at the stationary point. Because $\hat{\psi}_{n,A}$ and $\hat{\psi}_{n,B}$ are parallel at the stationary point. A similar reasoning can be applied to show that $\partial_m\partial_m(\hat{\psi}_{n,A}\hat{\psi}_{n,B}) = 0$.

C Stationary phase analysis

In this appendix an approximation for so called oscillatory integrals is derived. This type of integrals are written in the form

$$J = \oint_S A(\theta)e^{ik\Phi(\theta)}d\theta \tag{131}$$

with $A(\theta)$ and $\Phi(\theta)$ real-valued functions and S denoting the domain of integration. The behaviour of these integrals is investigated in the high frequency domain. The integrand in equation (131) is stationary with respect to θ when

$$\frac{d}{d\theta}\Phi(\theta) = 0. \tag{132}$$

For large $|k|$, $e^{ik\Phi(\theta)}$ oscillates rapidly for small changes in θ while $A(\theta)$ varies only slightly. Because of this, the integrand sums destructively everywhere except at the points where $\Phi(\theta)$ varies only slightly with changing θ, which occurs at the stationary points. The oscillating term sums constructively around a stationary point, and therefore the main contribution to the integral comes from the stationary points. Using this, the integral in equation (131) can be approximated by evaluating the integral around the stationary points and taking the sum over all stationary points

$$J \approx \sum_{n=1}^{N} J_n. \tag{133}$$

Where N is the total amount of stationary points on S and J_n the approximation of the integral around the n^{th} stationary point. To evaluate the integral a Taylor expansion of the phase term around a stationary point at θ_n is made according to

$$\Phi(\theta) = \Phi(\theta_n) + \frac{1}{2}\Phi''(\theta_n)(\theta - \theta_n)^2 + \mathcal{O}(\theta^3). \tag{134}$$

All terms of higher order than θ^2 are neglected. Also, note that $\Phi'(\theta_n) = 0$ and is therefore omitted from the Taylor series. Around the n^{th} stationary point J_n becomes

$$J_n = \int_{\theta_n-\varepsilon}^{\theta_n+\varepsilon} A(\theta)e^{ik(\Phi(\theta_n)+\frac{1}{2}\Phi''(\theta_n)(\theta-\theta_n)^2)}d\theta, \tag{135}$$

where ε is a sufficiently small positive number such that the Taylor expansion is valid within the domain of integration. Because $A(\theta)$ is nearly constant in the domain of integration, equation (135) becomes

$$J_n \approx A(\theta_n) e^{ik\Phi(\theta_n)} \int_{\theta_n-\varepsilon}^{\theta_n+\varepsilon} e^{\frac{1}{2}ik\Phi''(\theta_n)(\theta-\theta_n)^2} d\theta. \tag{136}$$

To evaluate the integral in equation (136) a change of variable is required. To this extent, two situations are considered; where $k\Phi''(\theta_n) > 0$ and where $k\Phi''(\theta_n) < 0$. To do so, define $u = \sqrt{\mu|k\Phi''(\theta_n)|}\,(\theta - \theta_n)$ such that $u^2 = \mu|k\Phi''(\theta_n)|(\theta-\theta_n)^2 = k\Phi''(\theta_n)(\theta-\theta_n)^2$ where $\mu = \mathrm{sgn}(k\Phi''(\theta_n))$. Because k is very large equation (136) becomes

$$J_n \approx \frac{A(\theta_n)e^{ik\Phi(\theta_n)}}{\sqrt{\mu|k\Phi''(\theta_n)|}} \int_{-\infty}^{\infty} e^{\frac{iu^2}{2}} du = \frac{A(\theta_n)e^{ik\Phi(\theta_n)}}{\sqrt{\mu|k\Phi''(\theta_n)|}} \sqrt{2i\pi}. \tag{137}$$

This can also be written as

$$J_n \approx \sqrt{\frac{2i\pi}{\mu|k\Phi''(\theta_n)|}} A(\theta_n) e^{ik\Phi(\theta_n)}. \tag{138}$$

Using $\frac{i}{\mu} = e^{\frac{i\pi}{2}} e^{-i\left(\frac{\pi}{2} - \frac{\mu\pi}{2}\right)} = e^{\frac{i\mu\pi}{2}}$ expression (138) can be rewritten as

$$J_n \approx e^{i\mu\frac{\pi}{4}} \sqrt{\frac{2\pi}{|k\Phi''(\theta_n)|}} A(\theta_n) e^{ik\Phi(\theta_n)}, \tag{139}$$

or

$$J_n \approx \sqrt{\frac{2\pi}{|k\Phi''(\theta_n)|}} A(\theta_n) e^{i\left(k\Phi(\theta_n) + \mu\frac{\pi}{4}\right)}. \tag{140}$$

The final result is a stationary phase approximation for integrals of the type shown in equation (131).

D Arbitrary domains

In this appendix it is shown that the result shown in equation (94) can also be obtained for more arbitrary domains and source and receiver configurations. The only assumption that is made here is that the medium is homogeneous and isotropic in a small region near the boundary $\partial\mathbb{D}$. For these media the largest contributions of $A(\hat{\phi}_A, \hat{\phi}_B)$ to the integral in equation (88) come from a stationary point where the ray angles $\alpha_A = \alpha_B \pm \pi$ or $\cos(\alpha_A) = -\cos(\alpha_B)$. In these stationary points, the directional derivatives in equation (89) can be approximated using $(\partial_i f(\mathbf{x}))n_i \approx -i\frac{\omega}{v_p}\cos(\alpha) f(\mathbf{x})$. It then becomes

$$\begin{aligned} A(\hat{\phi}_A, \hat{\phi}_B) = &-i\frac{\omega}{v_p}\big(\lambda\hat{\phi}_A(\partial_k\partial_k\hat{\phi}_B)\cos(\alpha_A) + 2\mu(\partial_i\hat{\phi}_A)(\partial_i\hat{\phi}_B)\cos(\alpha_B) \\ &- \lambda(\partial_k\partial_k\hat{\phi}_A)\hat{\phi}_B\cos(\alpha_B) - 2\mu(\partial_i\hat{\phi}_A)(\partial_i\hat{\phi}_B)\cos(\alpha_A)\big). \end{aligned} \tag{141}$$

Using $\cos(\alpha_A) = -\cos(\alpha_B)$ in the stationary point $A(\hat{\phi}_A, \hat{\phi}_B)$ becomes

$$A(\hat{\phi}_A, \hat{\phi}_B) = -i\frac{\omega}{v_p}\cos(\alpha_A)\big(\lambda\hat{\phi}_A(\partial_k\partial_k\hat{\phi}_B) + \lambda(\partial_k\partial_k\hat{\phi}_A)\hat{\phi}_B - 4\mu(\partial_i\hat{\phi}_A)(\partial_i\hat{\phi}_B)\big). \tag{142}$$

The P-wave potentials obey the scalar wave equation so that $\partial_k\partial_k\hat{\phi} = -\frac{\omega^2}{v_p^2}\hat{\phi}$. Using the scalar wave equation and the identity $\partial_i\partial_i(\hat{\phi}_A\hat{\phi}_B) = \hat{\phi}_A(\partial_i\partial_i\hat{\phi}_B) + \hat{\phi}_B(\partial_i\partial_i\hat{\phi}_A) + 2(\partial_i\hat{\phi}_A)(\partial_i\hat{\phi}_B)$ equation (90) can be rewritten as

$$A(\hat{\phi}_A, \hat{\phi}_B) = -i\frac{\omega}{v_p}\cos(\alpha_A)\big((\lambda+2\mu)\hat{\phi}_A(\partial_k\partial_k\hat{\phi}_B) + (\lambda+2\mu)(\partial_k\partial_k\hat{\phi}_A)\hat{\phi}_B - 2\mu\partial_k\partial_k(\hat{\phi}_A\hat{\phi}_B)\big) \tag{143}$$

or

$$A(\hat{\phi}_A, \hat{\phi}_B) = 2i\frac{\omega^3}{v_p^3}\cos(\alpha_A)(\lambda+2\mu)\hat{\phi}_A\hat{\phi}_B + 2i\frac{\omega}{v_p}\mu\partial_k\partial_k(\hat{\phi}_A\hat{\phi}_B). \tag{144}$$

It is shown in appendix B that $\partial_k \partial_k (\hat{\phi}_A \hat{\phi}_B) = 0$ at the stationary point, so

$$A(\hat{\phi}_A, \hat{\phi}_B) = 2i \frac{\rho \omega^3}{v_p} \cos(\alpha_A) \hat{\phi}_A \hat{\phi}_B \tag{145}$$

or

$$A(\hat{\phi}_A, \hat{\phi}_B) = -2\rho\omega^2 (\partial_i \hat{\phi}_A) \hat{\phi}_B. \tag{146}$$

Note that this result is the same as the result that is shown in equation (94). This shows that the simplification of the term $A(\hat{\phi}_A, \hat{\phi}_B)$ derived in section 4.3 is also valid in more arbitrary domains with other receiver configurations.

References

Aki, K. and Richards, P. G. (2002). *Quantitative seismology.* 2nd edition.

Bleistein, N. (1984). Mathematical methods for wave phenomena.

Boas, M. L. (2006). *Mathematical Methods in the Physical Sciences.* John Wiley & Sons., Inc, 3rd edition.

Curtis, A., Gerstoft, P., Sato, H., Snieder, R., and Wapenaar, K. (2006). Seismic interferometry—turning noise into signal. *The Leading Edge*, 25(9):1082–1092.

Dziewonski, A. M. and Anderson, D. L. (1981). Preliminary reference earth model. *Physics of the earth and planetary interiors*, 25(4):297–356.

Halliday, D. and Curtis, A. (2009). Seismic interferometry of scattered surface waves in attenuative media. *Geophysical Journal International*, 178(1):419–446.

Shapiro, N. M. and Campillo, M. (2004). Emergence of broadband rayleigh waves from correlations of the ambient seismic noise. *Geophysical Research Letters*, 31(7).

Slob, E., Draganov, D., and Wapenaar, K. (2007). Interferometric electromagnetic green's functions representations using propagation invariants. *Geophysical Journal International*, 169(1):60–80.

Wapenaar, K., Draganov, D., Snieder, R., Campman, X., and Verdel, A. (2010). Tutorial on seismic interferometry: Part 1—basic principles and applications. *Geophysics*, 75(5):75A195–75A209.

Wapenaar, K. and Fokkema, J. (2006). Green's function representations for seismic interferometry. *Geophysics*, 71(4):SI33–SI46.

Wapenaar, K., van der Neut, J., Ruigrok, E., Draganov, D., Hunziker, J., Slob, E., Thorbecke, J., and Snieder, R. (2011). Seismic interferometry by crosscorrelation and by multidimensional deconvolution: a systematic comparison. *Geophysical Journal International*, 185(3):1335–1364.